A PDF Dispersion Model for Buoyant Plumes in the Convective Boundary Layer

J. C. WEIL

Cooperative Institute for Research in Environmental Sciences, University of Colorado, and Visiting Scientist, National Center for Atmospheric Research, Boulder, Colorado*

L. A. CORIO AND R. P. BROWER

VERSAR, Incorporated, ESM Operations, Columbia, Maryland

(Manuscript received 5 August 1996, in final form 16 December 1996)

ABSTRACT

A probability density function (PDF) dispersion model is presented for buoyant plumes in the convective boundary layer (CBL), where the mean concentration field C is obtained from the PDFs p_y and p_z of tracer particle position in the lateral y and vertical z directions. The p_y is assumed to be Gaussian, whereas the p_z is derived from the the vertical velocity PDF, which is skewed. Three primary sources contribute to the modeled C field: 1) the ''direct'' or real source at the stack, 2) an ''indirect'' source to account for the slow downward dispersion of lofting plumes from the CBL top, and 3) a ''penetrated'' source to treat material that initially penetrates the elevated inversion but later fumigates into the CBL. Image sources are included to satisfy the zero-flux conditions at the ground and the CBL top.

Comparisons between the modeled crosswind-integrated concentration fields C^y and convection tank data show fair to good agreement in the lower half of the CBL. In particular, the C^y profiles at the surface agree with the data over a wide range of the dimensionless buoyancy flux F_* and show a systematic decrease in C^y with F_*.

Comparisons between the modeled and observed ground-level concentrations around several power plants exhibit good agreement on average and are considerably better than those obtained with a standard Gaussian plume model. A residual analysis suggests some areas for future model development.

1. Introduction

Over flat terrain, the maximum ground-level concentrations (GLCs) due to tall stack releases usually occur in a convective boundary layer (CBL). The high GLCs are caused by the large-scale convective updrafts and downdrafts that lead to a ''looping'' plume. For buoyant releases, plume sections can be brought to the surface within a few kilometers of the source when the downdraft velocity exceeds the rise velocity due to plume buoyancy. For sufficiently high buoyancy, a plume often rises to the top of the CBL, where it ''lofts,'' or remains temporarily, and then mixes downward. For yet higher buoyancy, a plume can penetrate the inversion capping the CBL, but later can be reentrained by the growing CBL, or ''mixed layer.''

Laboratory experiments by Willis and Deardorff (1983, 1987) demonstrated the complex dispersion patterns that can be obtained and their sensitivity to the source buoyancy flux, which was characterized by the dimensionless flux F_*:

$$F_* = \frac{F_b}{U w_*^2 z_i}, \tag{1}$$

where F_b is the stack buoyancy flux [Eq. (13a) below], U is the mean wind speed in the CBL, w_* is the convective velocity scale, and z_i is the CBL depth. Here, $w_* = (g\overline{w\theta_o} z_i/T_a)^{1/3}$, where g is the gravitational acceleration, $\overline{w\theta_o}$ is the surface kinematic heat flux, and T_a is the ambient absolute temperature. The laboratory experiments showed that the lofting behavior occurred for $F_* \gtrsim 0.1$. Field observations around power plant stacks (Hanna and Paine 1989; Weil et al. 1986) indicated that the maximum GLCs generally occurred for this F_* range, which typically existed during light and variable winds ($\lesssim$2 m s^{-1}) and low CBL depths ($\lesssim$500 m).

Over the past 15 years, our understanding of and modeling capability for dispersion in the CBL have improved substantially. The models that have been developed include 1) analytical–statistical approaches based on the probability density function (PDF) of the random vertical velocity w—the PDF model (Misra 1982; Venkatram 1983; Weil 1988), 2) Lagrangian sto-

* The National Center for Atmospheric Research is sponsored by the National Science Foundation.

Corresponding author address: Dr. Jeffrey C. Weil, NCAR/MMM, P.O. Box 3000, Boulder, CO 80307-3000.
E-mail: weil@ncar.ucar.edu

chastic models (Luhar and Britter 1989; Sawford and Guest 1987), 3) approaches based on second-order closure (Sykes et al. 1984, 1986), and 4) large-eddy simulations (Lamb 1982; Henn and Sykes 1992). The key advantages of the PDF model are its ability to capture the essential physics of dispersion and its relative simplicity, which make the model useful for air quality applications.

This paper focuses on a further development of the PDF model for the mean concentration field C due to buoyant plumes in the CBL. The concentration distribution in a plume is highly random and should be characterized not only by C, but also by the degree of randomness—for example, the root-mean-square concentration fluctuation σ_c (Sykes 1988). The PDF approach is amenable to the modeling of σ_c, but this is postponed for the future. Further information on concentration fluctuations can be found in Chatwin et al. (1995), Deardorff and Willis (1988), Hanna (1984), Henn and Sykes (1992), Mylne and Mason (1991), Sykes (1988), and Weil (1994); however, with a few exceptions, this work primarily addresses passive or nonbuoyant releases.

In the PDF approach, the mean concentration is found from the PDF of the tracer particle position, which in turn is derived from the w PDF. The model was applied first to passive scalar dispersion in the CBL (e.g., Misra 1982; Venkatram 1983; Weil 1988) and resulted in good agreement with the laboratory measurements of Willis and Deardorff (1978, 1981). In the CBL, the w PDF is positively skewed and results in a non-Gaussian vertical concentration distribution, which is included in the model. For buoyant plumes, the model was extended by superposing the displacements due to plume rise and the random w to obtain the concentration field (Weil et al. 1986). This approach worked well for weak to moderate buoyancy ($F_* < 0.1$), but for high F_* ($\gtrsim 0.1$), a separate treatment was required to account for the lofting behavior (see also Hanna et al. 1986; Weil 1988). However, the above separation did not maintain continuity of the predicted concentration field with F_*.

In this paper, we introduce a new and simplified treatment of plume interaction with the elevated inversion. This includes an ''indirect'' source to address the lofting behavior and dispersion of ''nonpenetrating'' plumes, and a ''penetrated'' source to account for plume material that initially penetrates the inversion but subsequently fumigates into the CBL (section 2). The treatment results in a continuous variation of C with F_*, thus overcoming a limitation of the earlier PDF models. In addition, we include the effects of surface shear as well as convection in parameterizing the w PDF, so that the model is applicable in the limit of a neutral boundary layer. The model is developed and evaluated using laboratory data and is compared to GLC observations around several Maryland power plants and the Kincaid (Illinois) power plant.

2. PDF dispersion model

The PDF model described here applies to an elevated point source in the CBL, wherein the turbulence is idealized as homogeneous and steady. The mean wind speed U is assumed to be uniform with height, and the lateral and vertical velocity fluctuations are assumed to be statistically independent. As a result, the displacements of source-emitted particles in the lateral y and vertical z directions, y_p and z_p, respectively, are independent. Thus, the joint PDF of y_p and z_p at time $t = x/U$ is given by $p_{yz}(y_p, z_p; x/U) = p_y(y_p; x/U)p_z(z_p; x/U)$, where x is the distance downwind of the source.

The ensemble-mean concentration $C(x, y, z)$ is found from a mass balance in which the mean horizontal flux of particles through an elemental area $\Delta y\Delta z$ normal to the mean wind is $UC(x, y, z)\Delta y\Delta z$. This is equal to the emission rate Q times the probability of particles lying in the intervals $y - \Delta y/2 < y_p < y + \Delta y/2$ and $z - \Delta z/2 < z_p < z + \Delta z/2$; the probability is given by $p_y(y_p; x/U)p_z(z_p; x/U)\Delta y\Delta z$. Thus, the mass balance can be expressed by $UC\Delta y\Delta z = Qp_yp_z\Delta y\Delta z$, or

$$C(x, y, z) = \frac{Q}{U}p_y\left(y; \frac{x}{U}\right)p_z\left(z; \frac{x}{U}\right), \tag{2a}$$

where we have set $y = y_p$ and $z = z_p$ in p_y and p_z.

In the Gaussian plume model, p_y has the familiar form

$$p_y = \frac{1}{\sqrt{2\pi}\sigma_y}\exp\left(-\frac{y^2}{2\sigma_y^2}\right), \tag{2b}$$

where $\sigma_y(x/U)$ is the crosswind spread, or standard deviation, and p_z has a similar form.

For the PDF model, the p_z is derived from the w PDF p_w, which is skewed, as noted earlier, and results in a non-Gaussian p_z; the p_y is assumed to be Gaussian (see Lamb 1982). In addition, the w in a downdraft or updraft is taken to be independent of z. A key assumption is that the Lagrangian timescale T_{Lz} for w is infinite, so that the particle velocity at any x downwind is uniquely determined by its initial velocity. This is an approximation that is partially justified by the large timescales ($z_i/w_* \sim 10$ min) of the CBL convection elements; the effect of a finite T_{Lz} is discussed in section 5.

In addition to the non-Gaussian p_z, the current model has the following features. 1) For buoyant releases, no ''final'' plume rise is assumed. Instead, the plume trajectories are determined by the addition of a distance-dependent plume rise (e.g., as $x^{2/3}$) and the random vertical displacement caused by w. GLCs appear when the downdraft velocities are sufficiently large to overcome the plume rise velocity. 2) For plume segments initially rising in updrafts, an indirect source is included above the CBL top to address the lofting behavior—that is, the plume tendency to remain near z_i and resist downward mixing. This source plays the same role as the first image source above z_i in the standard Gaussian model, but differs in the treatment of plume buoyancy.

3) A penetrated source, or plume, is included to account for material that initially penetrates the elevated inversion, but is subsequently reentrained by and disperses in the growing CBL.

Based on this discussion, there are three primary sources contributing to C: 1) the ''direct'' or ''real'' source (at the stack), 2) the indirect source, and 3) the penetrated source. In addition, image sources are included to satisfy the zero-flux conditions at $z = 0, z_i$. In the following, we discuss the treatment of each source including buoyancy effects as well as the concentration field. For convenience, we first obtain the crosswind-integrated concentration (CWIC) C^y and then find C from the assumed Gaussian form for p_y. The C^y is obtained by integrating Eq. (2a) over all y and gives

$$C^y(x, z) \equiv \int_{-\infty}^{\infty} C(x, y, z)\, dy = \frac{Q}{U} p_z. \tag{3}$$

a. Direct or real source

This source accounts for the surface CWIC and GLCs due to plume sections that reach the ground directly from the source via downdrafts.

1) Crosswind-integrated concentration

The PDF p_z of the particle height z_p can be found from p_w, provided that the z_p is a monotonic function of w (see Brownlee 1965). The relationship between p_z and p_w is (Weil 1988)

$$p_z = p_w\left[w\left(z_p; \frac{x}{U}\right)\right]\left|\frac{dw}{dz_p}\right|, \tag{4}$$

where the absolute value is taken to ensure that p_z is positive. Here, p_w represents a general form of the w PDF and will be taken below as skewed [Eq. (7)]. Writing the argument of p_w as $w(z_p; x/U)$ means that wherever w appears in p_w, we replace it by its equivalent in terms of z_p and x. The relationship between z_p and w is found by superposing the plume rise Δh and the vertical displacement due to w—that is, wx/U—as

$$z_p = h_s + \Delta h + \frac{wx}{U}, \tag{5}$$

where h_s is the stack height.

In Eq. (4), $w(z_p; x/U)$ is found by rearranging (5) as

$$w = (z_p - h_s - \Delta h)\frac{U}{x}, \tag{6}$$

from which we obtain $|dw/dz_p| = U/x$. This w and dw/dz_p are then substituted into Eq. (4) to obtain p_z.

In the CBL, a good approximation to the w PDF is the superposition of two Gaussian distributions (e.g., Baerentsen and Berkowicz 1984; Weil 1988),

$$p_w = \frac{\lambda_1}{\sqrt{2\pi}\sigma_{w1}} \exp\left[-\frac{(w - \overline{w_1})^2}{2\sigma_{w1}^2}\right] + \frac{\lambda_2}{\sqrt{2\pi}\sigma_{w2}} \exp\left[-\frac{(w - \overline{w_2})^2}{2\sigma_{w2}^2}\right], \tag{7}$$

where λ_1 and λ_2 are weighting coefficients for the distributions with $\lambda_1 + \lambda_2 = 1$. The $\overline{w_j}$ and σ_{wj} ($j = 1, 2$) are the mean vertical velocity and standard deviation for each distribution and are assumed to be proportional to σ_w, the ''total,'' or overall, root-mean-square vertical turbulence velocity; subscripts 1 and 2 denote the updraft and downdraft distributions, respectively. The $\overline{w_1}$, $\overline{w_2}$, σ_{w1}, σ_{w2}, λ_1, and λ_2 are found as functions of σ_w, the vertical velocity skewness $S = \overline{w^3}/\sigma_w^3$, where $\overline{w^3}$ is the third moment of w, and a parameter $R = \sigma_{w1}/\overline{w_1} = -\sigma_{w2}/\overline{w_2}$ (see appendix A). An alternative parameterization for $\overline{w_j}$ and σ_{wj} is discussed in section 5.

In our analysis of laboratory data, we find that $R = 1$ yields fair to good agreement between the modeled and measured CWIC fields (section 4a). However, for field observations, we choose $R = 2$, so that in the limit of a neutral boundary layer ($w_* = 0$) and an assumed $S = 0$, the PDF approximates a Gaussian PDF. (As Table 2 shows, there is little difference between the results for $R = 1$ and 2.)

In the upper 90% of the CBL, the vertical velocity variance σ_w^2 can be assumed to be uniform (Weil 1988), as can the skewness (Wyngaard 1988). Here, the σ_w^2 is parameterized in terms of w_* and u_* by

$$\sigma_w^2 = 1.2u_*^2 + 0.31w_*^2, \tag{8a}$$

where the 1.2 corresponds to Hicks's (1985) neutral limit ($w_* = 0$), and the 0.31 is consistent with Weil and Brower's (1984) convective limit ($u_* = 0$), or $\sigma_w/w_* = 0.56$. Similarly, the lateral velocity variance σ_v^2 can be assumed to be uniform over the CBL and parameterized by

$$\sigma_v^2 = 3.6u_*^2 + 0.31w_*^2, \tag{8b}$$

where the 3.6 is from Hicks and the 0.31 from Weil and Brower. In the convective limit, the S is taken to be 0.6, which is the vertically averaged value from the Minnesota experiments (Wyngaard 1988); the corresponding $\overline{w^3} = 0.6\sigma_w^3 = 0.105w_*^3$. For arbitrary u_* and w_*, the skewness is parameterized by $S = 0.105w_*^3/\sigma_w^3$, with σ_w^2 given by Eq. (8a); thus, as $w_* \to 0$, $S \to 0$, and for $w_*/u_* \gg 1$, $S = 0.6$.

Using the approach for finding p_z outlined above [Eqs. (4)–(6) and related discussion] and the p_w given by Eq. (7), we find the CWIC field for the direct plume to be

$$C_d^y(x, z) = \frac{Q}{\sqrt{2\pi}U}\left\{\frac{\lambda_1}{\sigma_{z1}} \exp\left[-\frac{(z - \Psi_1)^2}{2\sigma_{z1}^2}\right] + \frac{\lambda_2}{\sigma_{z2}} \exp\left[-\frac{(z - \Psi_2)^2}{2\sigma_{z2}^2}\right]\right\}, \tag{9a}$$

or

$$C_d^y(x, z) = \frac{Q}{\sqrt{2\pi}\,U} \sum_{j=1}^{2} \frac{\lambda_j}{\sigma_{zj}} \exp\left[-\frac{(z - \Psi_j)^2}{2\sigma_{zj}^2}\right], \quad (9b)$$

where

$$\sigma_{zj} = \frac{\sigma_{wj}x}{U} \quad \text{and} \quad \Psi_j = h_s + \Delta h + \frac{\overline{w_j}x}{U}, \quad \text{with } j = 1 \text{ or } 2. \quad (10)$$

To account for the zero-flux condition at the ground, we introduce an image source at $z = -h_s$—that is, we assume particle reflection at $z = 0$. This results in a positive flux of material at $z = z_i$, and additional image sources are included at $z = 2z_i + h_s$, $-2z_i - h_s$, etc., to satisfy the subsequent no-flux conditions at $z = z_i$, 0. The resulting CWIC due to the real and image sources is

$$C_d^y(x, z) = \frac{fQ}{\sqrt{2\pi}\,U} \sum_{n=0}^{N} \sum_{j=1}^{2} \frac{\lambda_j}{\sigma_{zj}} \times \left\{\exp\left[-\frac{(z - 2nz_i - \Psi_j)^2}{2\sigma_{zj}^2}\right] + \exp\left[-\frac{(z + 2nz_i + \Psi_j)^2}{2\sigma_{zj}^2}\right]\right\}, \quad (11)$$

where N is the number of image sources and f is the fraction of plume material that remains trapped in the CBL—that is, material that is unable to penetrate the elevated inversion. In section 4, N is taken as 50, which is more than adequate for the comparisons made there; a more computationally efficient choice for N can be made based on a series-convergence test. The expression for f is given in section 2c.

2) PLUME RISE

For the direct source, the plume rise is given by the superposition of the source momentum and buoyancy effects following Briggs (1975):

$$\Delta h = \left(\frac{3F_m x}{\beta_1^2 U^2} + \frac{3}{2\beta_1^2}\frac{F_b x^2}{U^3}\right)^{1/3}, \quad (12)$$

where F_m and F_b are the stack momentum and buoyancy fluxes, and β_1 (=0.6) is an entrainment parameter. The fluxes are defined by

$$F_m = \frac{\rho_s}{\rho_a} w_s^2 r_s^2 \quad \text{and} \quad F_b = g w_s r_s^2 \frac{\Delta T_s}{T_s}, \quad (13a)$$

where w_s, r_s, ρ_s, and T_s are the stack exit velocity, radius, density, and absolute temperature; ρ_a is the ambient density; and $\Delta T_s = T_s - T_a$. A dimensionless momentum flux (Weil 1994)

$$F_{m^*} = \frac{F_m}{U w_* z_i^2} \quad (13b)$$

is used for characterizing the source momentum flux in section 4.

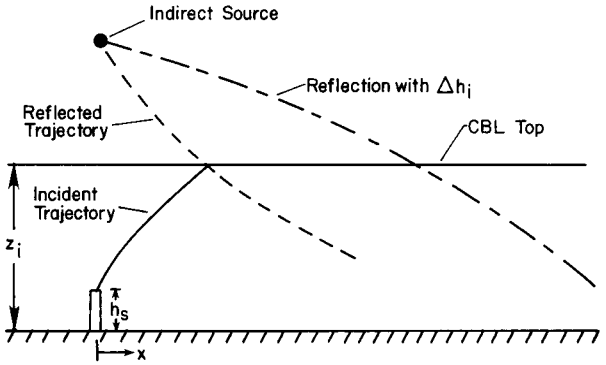

FIG. 1. Sketch of plume trajectory incident to the CBL top and reflected trajectories with and without Δh_i.

b. Indirect source

The indirect source is included to treat the *first* interaction of the ''updraft'' plume with the elevated inversion—that is, for plume sections that initially rise to the CBL top in updrafts, but are unable to penetrate the inversion and are returned to the ground via downdrafts. Image sources are added to treat the subsequent plume interactions with the ground and inversion and to satisfy the zero-flux conditions at $z = 0$, z_i. The treatment is designed to 1) provide for a continuous variation of C^y with F_* and 2) simplify computationally the analysis given in an earlier model (Hanna et al. 1986).

For the indirect source, a modified reflection approach is adopted in which the vertical velocity is reflected at $z = z_i$, but an ''effective'' plume rise Δh_i is added to delay the downward dispersion of plume material from the CBL top (see Fig. 1). This is intended to mimic the lofting behavior. The use of a reflection condition in the limit as $\Delta h \to 0$ is motivated by the results of Li and Briggs (1988) and Weil (1988), which showed this approach to be satisfactory for passive releases. The Δh_i is derived for the limiting case of a highly buoyant plume that intercepts the plane $z = z_i$ close to the source, but does not penetrate the inversion [section 2b(2)].

1) CROSSWIND-INTEGRATED CONCENTRATION

The mean CWIC due to the indirect source is found from Eq. (3), but with p_z corresponding to the reflected trajectories. In the latter, both the plume rise and the vertical velocity are reflected such that the resulting equation for z_p is

$$z_p = 2z_i - h_s - \Delta h - \frac{wx}{U} + \Delta h_i. \quad (14)$$

The corresponding $w(z_p; x/U)$ found by rearranging the above is

$$w = -(z_p - 2z_i + h_s + \Delta h_r)\frac{U}{x}, \qquad (15a)$$

where

$$\Delta h_r = \Delta h - \Delta h_i; \qquad (15b)$$

the Δh_i is discussed in section 2b(2). The above w and the $|dw/dz_p| = U/x$ are then substituted into Eq. (4) to obtain the p_z for the indirect plume. As Δh and Δh_i vanish, Eqs. (14) and (15a) reduce to the results for a passive release.

The CWIC due to the indirect source is found from p_z using Eqs. (4), (7), (14), and (15), and the related discussion. Image sources are included at $z = -2z_i + h_s$, $4z_i - h_s$, $-4z_i + h_s$, etc., to account for the zero flux at $z = 0$, z_i. The total CWIC due to these sources is

$$C_r^y(x, z) = \frac{fQ}{\sqrt{2\pi}U}\sum_{n=1}^{N}\sum_{j=1}^{2}\frac{\lambda_j}{\sigma_{zj}} \times \left\{\exp\left[-\frac{(z - 2nz_i + \Psi_j)^2}{2\sigma_{zj}^2}\right] + \exp\left[-\frac{(z + 2nz_i - \Psi_j)^2}{2\sigma_{zj}^2}\right]\right\}, \qquad (16)$$

where

$$\Psi_j = h_s + \Delta h_r + \frac{\overline{w_j}x}{U}, \quad \text{with} \quad j = 1 \text{ or } 2, \qquad (17)$$

and σ_{zj} is given by Eq. (10). Note that in the exponential terms of Eq. (16), the variables $2nz_i$ and Ψ_j are of opposite sign, whereas they are of the same sign in Eq. (11).

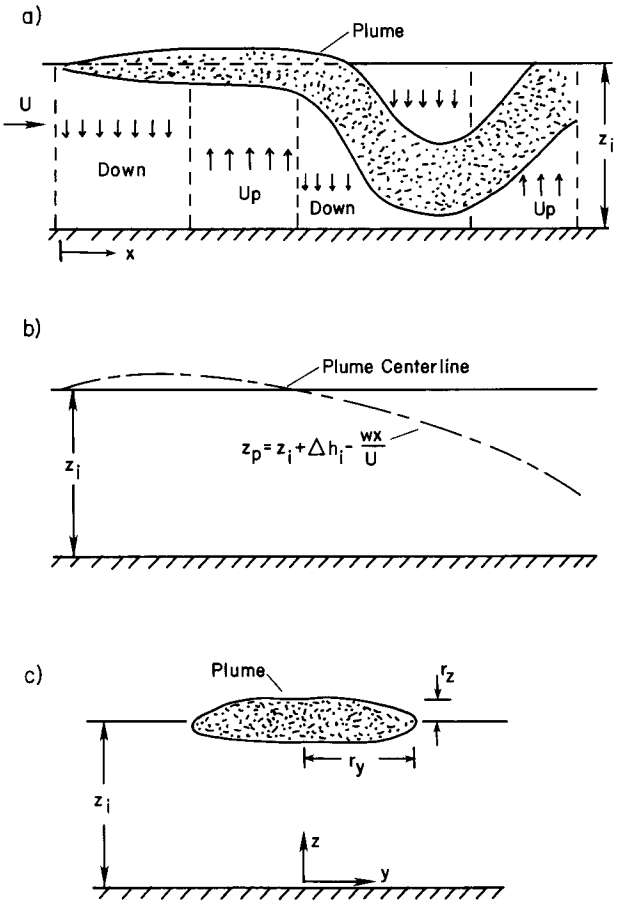

FIG. 2. Schematic showing the lofting plume: (a) behavior in the CBL, (b) trajectory for a single random velocity w, and (c) cross section at the CBL top.

2) AN EFFECTIVE PLUME RISE

For the indirect plume, an effective plume rise Δh_i is found using a simple energy argument governing the descent of buoyant plume elements from the CBL top. The plume is imagined to behave as a stable density interface subjected to convective mixing from below, akin to the entrainment of air above the density jump at the top of the CBL. Plume elements are assumed to be carried to the surface by downdrafts (Fig. 2a). For an element with an initial height $z_p = z_i$, initial vertical velocity $-w$, and no further entrainment of ambient air, the element's vertical velocity and trajectory are given by

$$w_p = -w + g't \qquad (18a)$$

and

$$z_p = z_i - wt + \frac{1}{2}g't^2, \qquad (18b)$$

where $g' = g\Delta\rho/\rho_a$, $\Delta\rho = \rho_a - \rho$, and ρ is the plume density when an element begins its downward displacement.

If we assume that the plume element has a zero vertical velocity when it reaches the surface—$w_p = 0$ at $z_p = 0$—the time required for this displacement to occur is $t = w/g'$ [see Eq. (18a)]. The corresponding w for the displacement is found by substituting this t and $z_p = 0$ into (18b); the result is $w^2/2 = g'z_i$. We use the last result as the basic criterion governing the onset of the plume parcel displacement from the CBL top, but modify it by the constant α as below:

$$\alpha\frac{\rho_a w^2}{2} = \Delta\rho g z_i \quad \text{or} \quad w = \left(\frac{2g'z_i}{\alpha}\right)^{1/2}. \qquad (19)$$

Here, $\Delta\rho$ is found from the buoyancy flux F_b and the relative dispersion of the elevated plume, as discussed below. A simple estimate of α (=1.4) is obtained by applying the model to the negative heat or buoyancy flux at the top of the CBL (appendix B).

The Δh_i can be found by requiring that a plume element enter the CBL at the distance where the criterion given by (19) is satisfied. For a plume originating at the CBL top, the trajectory for plume elements carried by downdrafts is

$$z_p = z_i + \Delta h_i - \frac{wx}{U}. \tag{20}$$

Assuming that the source buoyancy initially dominates in (20), z_p initially exceeds z_i, but becomes less than z_i some distance downwind as the downdraft speed overcomes the buoyancy effect (Fig. 2b). The trajectory intersects the height $z = z_i$ when $\Delta h_i = wx/U$. Substituting w given by (19) into the Δh_i expression, we obtain

$$\Delta h_i = \left(\frac{2g'z_i}{\alpha}\right)^{1/2}\frac{x}{U}. \tag{21}$$

The density deficit in (21) can be estimated from the F_b and the local plume spread, or relative dispersion, which is a function of x. For this purpose, we consider a plume with an elliptical cross section having an enhanced lateral spread r_y and a diminished vertical spread r_z (Fig. 2c). For a plume trapped in the CBL, the local buoyancy flux F is conserved and given by

$$F = F_b = Ur_y r_z \frac{g\Delta\rho}{\rho_a}. \tag{22}$$

Substituting Eq. (22) into Eq. (21), we have

$$\Delta h_i = \left(\frac{2F_b z_i}{\alpha U r_y r_z}\right)^{1/2}\frac{x}{U}. \tag{23}$$

The above model can be completed upon specifying the half-widths, r_y and r_z, of the plume cross section. For this, we use a modified version of an entrainment model (Weil 1991) for plumes lofting at the CBL top (see appendix C). The model gives

$$r_y r_z = r_i^2 + \frac{a_e \alpha_y^{3/2}}{4}\frac{w_*^2 x^2}{U^2}, \tag{24}$$

where $r_i = \beta_2(z_i - h_s)$ is the plume radius when the plume reaches the CBL top, $\beta_2 = 0.4$, $\alpha_y = 2.3$, and a_e is a dimensionless entrainment parameter, which is empirically estimated to be 0.1 (section 4a).

c. Penetrated source

The penetrated source was omitted initially, but a number (14) of high-GLC cases were found at the Kincaid plant when complete penetration or $f = 0$ was predicted, thus resulting in a zero prediction of the GLC. This typically occurred with low z_i values, $z_i \leq 300$ m, and light winds. The following model is a simple ad hoc approach to deal with this problem, primarily at the Kincaid plant, and will be revised or generalized in the future.

1) CROSSWIND-INTEGRATED CONCENTRATION

We first consider the limit of complete penetration, or $f = 0$. The plume is assumed to be entrained into the CBL by a growing z_i—that is, a fumigation process.

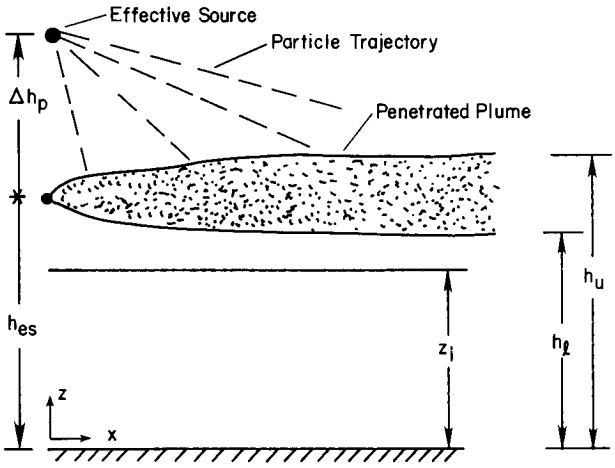

FIG. 3. Schematic of penetrated plume and treatment of its dispersion using a single effective point source.

Thus, the problem is unsteady in reality, but we treat it as steady in order to obtain a simple CWIC expression.

As shown by Deardorff and Willis (1982), plume fumigation into a growing CBL is not instantaneous, but occurs over a ''fumigation period'' t_f due to the horizontal variability of the entrainment layer. From their convection tank experiments, Deardorff and Willis found that the dimensionless t_f, or T_f, could be parameterized by

$$T_f = \frac{t_f w_*}{z_i} = \frac{0.42\Delta z_i/z_i}{w_e/w_*} + 2.3, \tag{25}$$

where Δz_i is the variability in the mixed layer height and w_e is the entrainment velocity at $z = z_i$. Deardorff and Willis also found that $\Delta z_i/z_i$ could be approximated by

$$\frac{\Delta z_i}{z_i} = 0.2 + 4\frac{w_e}{w_*}. \tag{26}$$

Substituting Eq. (26) into Eq. (25), we find the T_f to be

$$T_f = \frac{0.084}{w_e/w_*} + 4. \tag{27}$$

In the following, we adopt a point source at height h_p as a crude representation of dispersion from the penetrated source (Fig. 3). We account for the longitudinal distance $x_f = Ut_f$, or spread over which a quantity of material would be entrained into the CBL, and model this spread by locating the source at a height Δh_p above the stabilized plume height h_{es} [section 3b(2)]; thus, $h_p = h_{es} + \Delta h_p$. All material dispersing from the penetrated source is assumed to be passive and to occur via downdrafts. The Δh_p is obtained by assuming that the mean centerline of the downdraft plume passes through the point $(x, z) = (x_f/2, h_{es})$. Thus, we have $x_f/2 = Ut_f/2 = U\Delta h_p/|\overline{w_2}|$, or

$$\Delta h_p = \frac{|\overline{w_2}| t_f}{2}. \tag{28}$$

Penetrated source material is assumed to be mixed into the CBL only when the growing, time-dependent CBL height $\tilde{z}_i > z_i$, where z_i is the average mixed layer depth over the hour and is representative of the midpoint of the hour. The $\tilde{z}_i$ is obtained from Carson's (1973) model as

$$\tilde{z}_i^2 = z_i^2 + \frac{1 + 2A}{\partial\Theta_i/\partial z} \int_0^{t'} \frac{Q_o\, dt}{\rho_a c_p}, \tag{29}$$

where t' is measured from the midpoint of the hour, $\partial\Theta_i/\partial z$ is the potential temperature gradient for $z > z_i$, and A (=0.2) is the ratio of the heat flux at $z = z_i$ to that at the surface (see Moeng and Wyngaard 1989). The penetrated plume is assumed to be dispersed in the average CBL depth over the second half of the hourly period, $\tilde{z}_{i1} = \tilde{z}_i(t_1')$, with $t_1' = 15$ min.

With the above assumptions, the CWIC due to the penetrated source is given by

$$C_p^y(x, z) = \frac{f_p Q}{\sqrt{2\pi}\, U} \sum_{n=0}^{N} \sum_{j=1}^{2} \frac{\lambda_j}{\sigma_{zj}} \times \left\{ \exp\left[-\frac{(z - 2n\tilde{z}_{i1} - \Psi_j)^2}{2\sigma_{zj}^2} \right] + \exp\left[-\frac{(z + 2n\tilde{z}_{i1} + \Psi_j)^2}{2\sigma_{zj}^2} \right] \right\}, \tag{30}$$

where

$$\Psi_j = h_p + \frac{\overline{w_j} x}{U}, \quad \text{with} \quad j = 1 \text{ or } 2,$$

and

$$f_p = (1 - f)\frac{f_t f_q}{f_d}. \tag{31}$$

Here, $1 - f$ is the fraction of the source material that is in the penetrated plume, f_d (~0.6) is the fraction of the w PDF comprised by downdrafts, f_t (=0.5) is the fraction of the hourly period over which the penetrated source contributes to the GLCs, and f_q is the fraction of the penetrated plume that is captured by the growing CBL during the second half of the hour.

The f_q is given by

$$f_q = \min\left(\frac{\tilde{z}_{i2} - h_l}{h_u - h_l}, 1 \right), \tag{32}$$

where $\tilde{z}_{i2} = \tilde{z}_i$ ($t' = 30$ min) is the CBL height at the end of the hour, and h_l and h_u are the lower and upper heights of the penetrated plume (see Fig. 3).

2) Plume rise and inversion penetration

The fraction of the source material that remains in the CBL is given by $f = 1 - P$, where P is the fraction that penetrates the inversion. Adopting the P given by Briggs (1984), we find the f to be

$$f = \begin{cases} 0, & z_i' < 0.5\Delta h_{\text{eq}}, \\ 1, & z_i' > 1.5\Delta h_{\text{eq}}, \\ \dfrac{z_i'}{\Delta h_{\text{eq}}} - 0.5, & 0.5\Delta h_{\text{eq}} < z_i' < 1.5\Delta h_{\text{eq}}, \end{cases} \tag{33}$$

where

$$z_i' = z_i - h_s, \qquad \Delta h_{\text{eq}} = 2.6\left(\frac{F_b}{U N_i^2} \right)^{1/3},$$

and

$$N_i = \left(\frac{g}{\Theta_a} \frac{\partial\Theta_i}{\partial z} \right)^{1/2}. \tag{34}$$

The Δh_{eq} is the equilibrium plume rise in a stable environment (see Briggs 1984).

Briggs's model for P is based on a uniform rectangular plume cross section and a total vertical plume depth equal to Δh_{eq}. We assume that the plume height h_{es} is the centroid of the plume material above the inversion and take $h_{es} = h_s + \Delta h_{\text{eq}}$ for $f = 0$ or complete penetration. However, for partial penetration ($f > 0$), h_{es} is taken as the average of the heights of the upper plume edge $h_s + 1.5\Delta h_{\text{eq}}$ and z_i, or

$$h_{es} = \frac{h_s + z_i}{2} + 0.75\Delta h_{\text{eq}}. \tag{35}$$

d. Ground-level concentrations and lateral dispersion

The mean concentration field along the plume centerline ($y = 0$) can be found from the CWIC field through $C(x, 0, z) = C^y(x, z)/\sqrt{2\pi}\sigma_y$. For the "three-plume" contribution, we estimate the GLC along $y = 0$ by summing the contributions from the individual plumes according to

$$C(x, 0, 0) = \frac{1}{\sqrt{2\pi}} \left(\frac{C_d^y}{\sigma_{yd}} + \frac{C_r^y}{\sigma_{yr}} + \frac{C_p^y}{\sigma_{yp}} \right). \tag{36}$$

Here, σ_{yd}, σ_{yr}, and σ_{yp} are the lateral dispersion parameters for the direct, indirect, and penetrated plumes, and are discussed below.

For the direct plume, the lateral dispersion is assumed to be dominated by ambient turbulence, with σ_{yd} parameterized by the general form $\sigma_{yd} = \sigma_v t\,(1 + 0.5t/T_{Ly})^{-1/2}$ (e.g., Venkatram 1988), which satisfies the short- and long-time limits of Taylor's (1921) theory. With the σ_v given by Eq. (8b), the σ_{yd} is

$$\sigma_{yd} = \frac{(3.6u_*^2 + 0.31w_*^2)^{1/2}(x/U)}{[1 + 0.5x(UT_{Ly})^{-1}]^{1/2}}. \tag{37}$$

We adopt $T_{Ly} = 0.7z_i/w_*$ following Weil and Corio (1985), who found that Eq. (37), with this T_{Ly} and u_*

TABLE 1. Range of stack conditions, meteorological variables, and ground-level concentrations at power plants used in model evaluation.

	Maryland plants	Midwest plants	Kincaid plant
Stack height (m)	122–213	107–305	187
Stack emission rate	0.7–4 kg s^{-1} SO_2	3.9–10.5 kg s^{-1} SO_2	10–25 g s^{-1} SF_6
Buoyancy flux per stack (m^4 s^{-3})	125–772	516–2206	500–2400
Mean wind speed (m s^{-1})	0.7–15.7	0.4–2.6	2–16
CBL height (m)	300–2500	1000–1300	200–2500
Ground-level concentration	4–322 ppb SO_2	150–560 ppb SO_2	1–670 ppt SF_6
Distance to concentration (km)	1.7–33	1.3–1.8	0.5–50
Number of measurements	136	9	302

$= 0$, was a good average fit to the σ_y of buoyant plumes at Maryland power plants.

The indirect source treats plumes that rise to the CBL top in updrafts and loft. Such plumes exhibit an enhanced σ_y in the form of a gravity current due to the pressure difference between the plume and the local environment (Briggs 1985); the pressure difference is caused by the density difference $\Delta\rho$. For $F_* > 0.06$, Briggs found that σ_y was described by the following expression, which we adopt as an upper bound for σ_{yr}:

$$\sigma_{yr} = 1.6\frac{F_b^{1/3}}{U}x^{2/3}. \tag{38}$$

For weakly buoyant plumes, the CBL turbulence may dominate the lateral dispersion and lead to the σ_{yr} given by Eq. (37). As a simple approach for determining the applicability of these two expressions, we equate them at an $x = Uz_i/w_*$ and solve for the buoyancy flux at which the expressions are equal. The dimensionless buoyancy flux F_{*1} corresponding to this equality is

$$F_{*1} = \left[0.07 + 0.83\left(\frac{u_*}{w_*}\right)^2\right]^{3/2}. \tag{39}$$

Thus, we use Eq. (37) for $F_* < F_{*1}$, setting $\sigma_{yr} = \sigma_{yd}$, and Eq. (38) for $F_* \geq F_{*1}$.

For the penetrated plume, we currently assume that $\sigma_{yp} = \sigma_{yr}$ and will examine this further in the future.

3. Field data

a. Experimental description

The field data used in the model evaluation consisted of GLCs of stack effluents, meteorological variables, and stack conditions from buoyant sources—Maryland power plants and the Kincaid power plant. The Maryland plants—Chalk Point, Dickerson, and Morgantown—were in remote areas and far from other sources of SO_2 that the tracer monitored. Crosswind profiles of SO_2 were measured from a mobile instrumented van, which made repeated passes through the plume along roads transverse to the plume centerline. Typically, six profiles were measured along the same route during a 1-h interval and from them, an Eulerian-averaged profile was constructed. The maximum concentration from the average profile was used in the model evaluation.

The meteorological variables included vertical profiles of wind from balloon tracking and vertical temperature profiles from radiosondes or instrumented aircraft. These data were supplemented by surface observations—wind speed, cloud cover, and ceiling height—from the Washington National and Dulles International Airports. In addition, insolation data were obtained from Dulles Airport for estimating the surface heat flux.

Eleven additional SO_2 measurements were obtained during light wind, convective conditions from fixed monitors close ($x < 3$ km) to four power plants—Morgantown, Muskingum River (Ohio), John Sevier (Tennessee), and Cumberland (Tennessee).

The Kincaid plant is located in flat farmland near Springfield, Illinois. Continuous releases of SF_6 from the 187-m stack were made in approximately 30 experiments, each over a period of about 6–9 h. Hourly averaged SF_6 GLCs were measured at 200 sampling stations arranged on approximately five to seven arcs and ranging from 0.5 to 50 km downwind of the source.

The meteorological data included wind speed, wind direction, and temperature at four levels on a 100-m tower near the stack. These data were supplemented by vertical profiles of wind and temperature from rising instrumented balloons. In addition, hourly values of net radiation, insolation, and cloud cover were measured at the site. The SF_6 emission rate and other stack exit conditions were obtained either from in-stack monitors or plant operating data.

The ranges of stack conditions, meteorological variables, and GLC data from the various plants are shown in Table 1. Further experimental details can be found in Weil and Brower (1984) for the Maryland plants and in Hanna and Paine (1989) for the Kincaid plant.

b. Meteorological inputs and GLC data

The PDF model requires several key meteorological variables—the surface heat flux $Q_o = \rho_a c_p \overline{w\theta_o}$, where c_p is the specific heat of air, z_i, U, and u_*; the w_* is determined from Q_o and z_i. The variables are given by Weil and Brower (1984) for the Maryland plants and

Hanna et al. (1986) for the Kincaid plant. The methods for determining the variables differ somewhat for the two sites and are briefly summarized below.

- For the Maryland plants, Q_o was assumed to be $0.4Q_r$ (Weil and Brower 1984), where Q_r is the insolation. For the Kincaid plant, Q_o was estimated from the Holtslag and van Ulden (1983) model using the observed Q_r and an assumed moisture coefficient of 0.5 in their model. The Holtslag and van Ulden model generally gave similar results to $Q_o = 0.4Q_r$, but with slightly less variability.
- The z_i was determined from the observed temperature profiles and was subjectively chosen as the height at which the vertical temperature gradient first became isothermal above a ground-based, well-mixed layer. It was interpolated with time between the observed profiles using a modified version of Carson's (1973) model (Weil and Brower 1983), which is based on an energy balance of the CBL.
- For the Maryland plants, the U was a vertically averaged value from the balloon-tracked wind profiles. For the Kincaid plant, U was obtained by extrapolating the 10-m-level wind speed [$\bar{u}(z = 10$ m)] to the height $0.1z_i$ using the Monin–Obukhov (M–O) similarity profile (e.g., see Businger 1973):

$$\bar{u}(z) = \frac{u_*}{k}\left[\ln\left(\frac{z}{z_o}\right) - \psi_m\left(\frac{z}{L}\right)\right], \tag{40}$$

  where k is the von Kármán constant (0.4), z_o is the roughness height, ψ_m is a stability function, and L is the M–O length; $L = -u_*^3(kg\overline{w\theta_o}/T_a)^{-1}$. The $\bar{u}(0.1z_i)$ has been shown to give good estimates of the mean wind speed in the CBL (e.g., Garrett et al. 1982; Weil and Brower 1983).
- For Kincaid, the u_* was evaluated iteratively from Eq. (40) using the observed 10-m-level wind speed, $z_o = 0.15$ m, and the calculated Q_o. For the Maryland plants, u_* was estimated with less precision as $U/16$. The latter is a simple estimate based on the logarithmic wind profile applied at heights of 100–300 m for $z_o = 0.3$ m (see Briggs 1975; his Table 6); this z_o is typical of the power plant sites that are located in rolling terrain with patches of farmland and trees. On-site surface winds were not measured at the Maryland plants.

The observed GLCs' C_{obs} used in the model evaluation were the maximum concentrations from the average crosswind profiles in the Maryland experiments and the maxima on crosswind arcs in the Kincaid experiments. The Kincaid GLC data were screened to eliminate uncertain SF_6 concentrations, cases in which the plume centerline concentration was poorly defined by the sampling arc, and periods with low and ill-defined Q_o. The specific criteria that had to be satisfied were (see Hanna et al. 1986; appendix C)

- $C_{\text{obs}} > 10$ ppt, where the latter value is an uncertainty in the SF_6 concentration based on replicate samples and performance audits (Bowne et al. 1983);
- the observed peak concentration had to lie within an arc of $\pm 2\sigma_v/U$ centered about the expected plume direction, which was chosen as the wind direction at the 100-m level on the Kincaid tower; and
- the Q_o had to exceed 60 W m^{-2}, and the comparisons were restricted to days without rain.

4. Model comparisons with experimental data

This section focuses on the model performance using both laboratory data and field observations.

a. Laboratory experiments

The laboratory data were obtained from experiments conducted in a convection tank using water as the working fluid (Deardorff and Willis 1984, 1988; Willis and Deardorff 1987). A model stack was towed across the bottom of a simulated CBL, which had a mean z_i in the different experiments ranging from 19 to 23 cm and a $w_* = 0.9$ cm s^{-1}. For the following data, $h_s/z_i = 0.13$ or 0.16, and the F_* and F_{m*} were in the ranges $0 \le F_* \le 0.54$ and $0.001 \le F_{m*} \le 0.0058$.

The σ_w and skewness S used in the model were guided by the Deardorff and Willis (1985) turbulence measurements in the same tank. Their data showed that the vertically averaged $\sigma_w^2/w_*^2 \simeq 0.29$ or $\sigma_w/w_* \simeq 0.54$, which is close to the parameterized value 0.56 from Eq. (8a) for convective turbulence only; as a result, we used the parameterized value. The vertically averaged S was 1 for $0 < z/z_i < 0.5$ (i.e., in the near-source region), and $S = 1$ was used in the following calculations; this is somewhat larger than the vertically averaged S (=0.6) based on field observations (Wyngaard 1988).

To implement the model, we determine values of the entrainment parameter a_e [Eq. (24)] and the PDF variable R (appendix A) using model comparisons with the measured surface CWIC distribution. The CWIC in this and the following comparisons is shown as a function of the dimensionless distance

$$X = \frac{w_* x}{U z_i}, \tag{41}$$

which is the ratio of travel time x/U to the eddy turnover time z_i/w_*.

Figure 4 shows the dimensionless CWIC ($C^y U z_i/Q$) versus X for a low- ($F_* = 0.03$) and a high- ($F_* = 0.26$) buoyancy case, each for a range of a_e and two R values. In both cases, the modeled CWIC agrees well with the laboratory data for $R = 1$ and exhibits little variation with a_e over the range $0.05 \le a_e \le 0.2$. An $a_e = 0.1$ is an adequate fit to the data and is adopted in all of the remaining calculations. For $F_* = 0.03$, the results with $R = 1$ are a better match to the measurements than with $R = 2$, but for $F_* = 0.26$, there is little

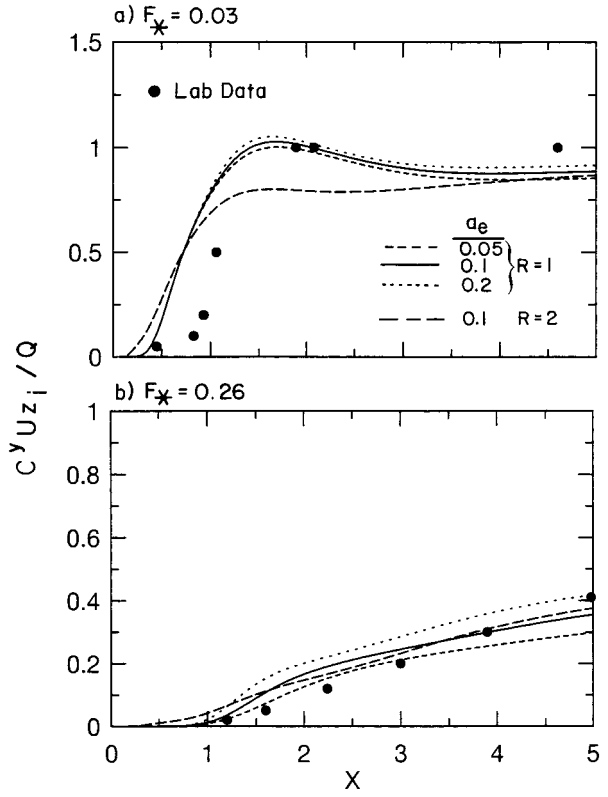

FIG. 4. Surface values of the dimensionless crosswind-integrated concentration as a function of the dimensionless downwind distance as predicted by the PDF model (lines) and measured in experiments with $h_s/z_i = 0.16$. Laboratory data are from (a) Deardorff and Willis (1988), with $F_{m*} = 0.0014$, and (b) Willis and Deardorff (1987), with $F_{m*} = 0.0058$.

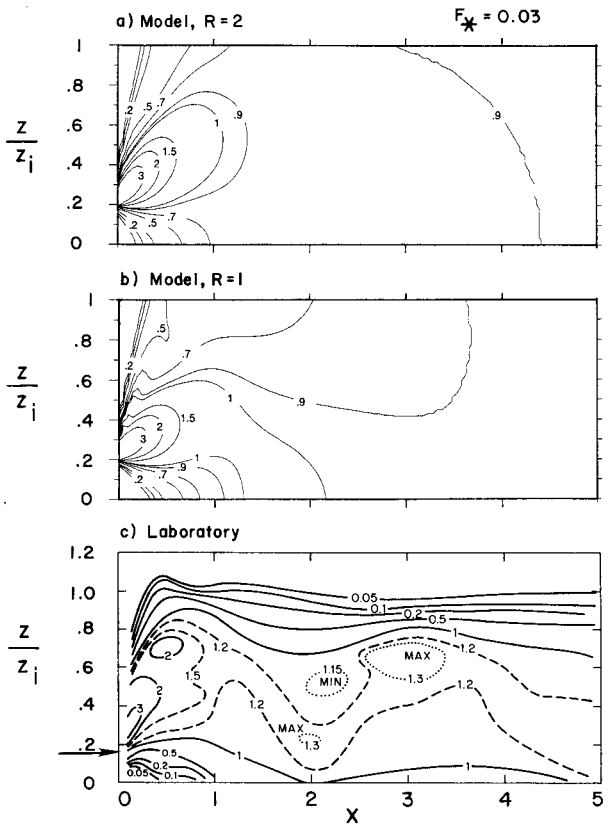

FIG. 5. Contours of the dimensionless crosswind-integrated concentration as a function of the dimensionless height and downwind distance for a buoyant source in the convective boundary layer, with $h_s/z_i = 0.16$ and $F_{m*} = 0.0014$; CWIC is nondimensionlized by Q/Uz_i. Laboratory results in (c) are from Deardorff and Willis (1988), and horizontal arrow denotes source height.

difference in the results for the two R values. The comparisons for the other high-buoyancy cases ($F_* = 0.11$, 0.14, and 0.54) are similar to those in Fig. 4b.

Figures 5 and 6 show contours of the dimensionless CWIC as a function of z/z_i and X for $F_* = 0.03$ and 0.14. Each figure contains the modeled contours for $R = 1$ and 2, and the laboratory measurements. With $R = 1$, both figures (Figs. 5b and 6b) show an overall qualitatively similar pattern to the laboratory data in the near field, say $X \lesssim 2$. For example, there is an upward tilting of the contour lines due to the plume rise, and as expected, the effect is more pronounced for the higher buoyancy flux (Fig. 6b). The upward tilting differs from the behavior for passive plumes ($F_* = F_{m*} = 0$), which exhibit downward-tilting contours due to the positive skewness or the higher probability (0.6) of material being released into downdrafts than into updrafts (Lamb 1982; Weil 1988). In Fig. 5b, the contours labeled ''1'' ($C^yUz_i/Q = 1$) initially rise over the region $X \lesssim 1$ and then descend to the surface in a manner similar to the 1 and 1.2 contours in the laboratory (Fig. 5c). This behavior is not found with $R = 2$ (Fig. 5a); thus, we conclude that the results for $R = 1$ are a better match with the laboratory data.

In contrast to the laboratory results, which show approximately horizontal contour lines near $z/z_i = 1$, the modeled contours are nearly normal to the lower and upper boundaries. The laboratory behavior is expected for buoyant material, which initially penetrates the inversion (near $X \sim 0.5$ in Figs. 5 and 6) and either returns to the CBL due to insufficient buoyancy or remains penetrated. The modeled behavior differs from this due to the assumed reflection ($z = 0$) or quasi reflection ($z = z_i$) of particles at the boundaries; the assumption is a better approximation at the surface than at the CBL top. As a result, we consider the model to be a dispersion parameterization primarily for the lower half or so of the CBL and in particular for the ground-level distribution of C^y and C.

Figure 7 compares the modeled CWIC at the surface with the data for six F_* values. In all calculations, $R = 1$, and for high F_* (Figs. 7d–f), the f [see Eq. (11)] is an experimental value at $X = 5$ taken from Willis and Deardorff (1987, their Fig. 10).

Overall, the predicted CWIC profiles are in fair to good agreement with the data, and in particular, they show a systematic reduction in the surface CWIC with

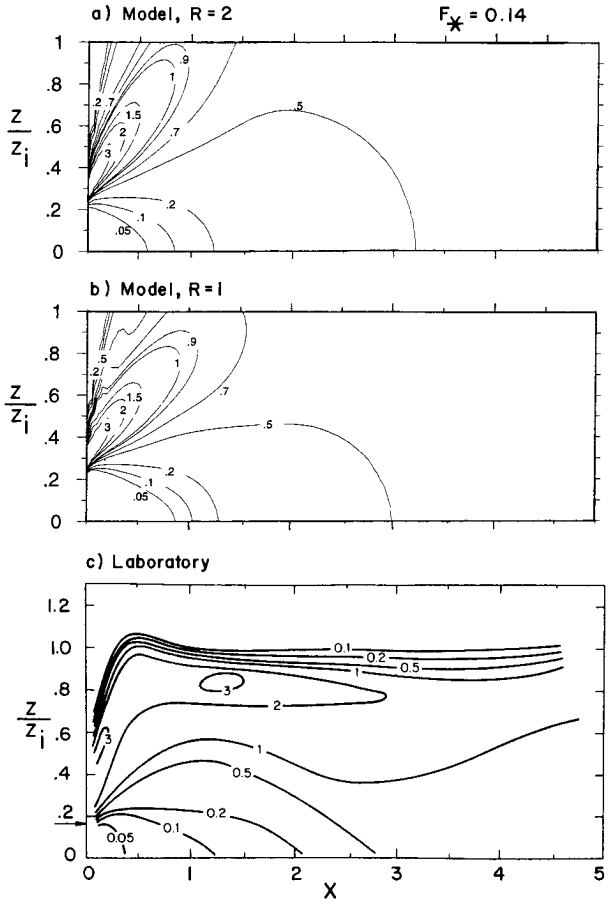

FIG. 6. Contours of the dimensionless crosswind-integrated concentration as a function of the dimensionless height and downwind distance for a buoyant source in the convective boundary layer, with $h_s/z_i = 0.16$ and $F_{m*} = 0.0058$; CWIC is nondimensionlized by Q/Uz_i. Laboratory results in (c) are from Willis and Deardorff (1987), and horizontal arrow denotes source height.

increasing F_*, as observed. The largest discrepancies between the model and experiments occur for the nonbuoyant plumes (Fig. 7a), but they are not systematic with respect to the momentum flux. For $F_{m*} = 0.001$, the model peaks at the correct distance, but it underestimates the magnitude of the peak, whereas for $F_{m*} = 0.0058$, the model overestimates the measured peak. However, in both cases, the large distance asymptote $C^yUz_i/Q = 1$, characteristic of a vertically well-mixed plume, is adequately represented.

In summary, we have found that the PDF model gives a fair to good representation of the dispersion pattern in the lower half of the CBL and of the surface CWIC distribution with X. Further work is necessary to improve the modeled behavior in the upper half of the CBL, particularly near $z = z_i$.

b. Field observations

To further evaluate the model, we compare the predicted centerline GLCs with the maximum SF_6 and SO_2 GLCs from observed crosswind profiles near the Kincaid and Maryland power plants. The model results are based on the following parameter values: $a_e = 0.1$, $R = 2$ [see section 2a(1)], σ_w and σ_v given by Eqs. (8a) and (8b), $S = 0.105w_*^3/\sigma_w^3$, and a default value of $\partial\Theta_i/\partial z = 0.005$°C m^{-1} in the elevated stable layer ($z > z_i$). The model sensitivity to some of the parameters (Table 2) is discussed later. A total of 302 and 145 GLC observations are analyzed in the Kincaid and Maryland datasets.

Before discussing the concentration estimates, we compare the observed and predicted σ_y at the Maryland plants. For comparison purposes, we assume that the predicted σ_y can be given by Eq. (37) for $F_* < 0.1$ and by Eq. (38) for $F_* \geq 0.1$ (e.g., see Weil et al. 1986); this is done because the modeled σ_y is given separately for the direct and indirect sources. Figure 8 shows that the observations and predictions generally agree to within a factor of 2. In addition, a least squares fit to the data (dashed line) does not vary significantly from the line of equal values (solid line) over the range of the predictions.

Following the recommendations of Fox (1984), Venkatram (1982), and Weil et al. (1992), we examine the correlation between the observed (C_{obs}) and predicted (C_{pred}) concentrations, normalized here by Q, and then analyze the residual, or difference d, between the concentrations. The normalization by Q is included to remove the variability in C due to varying emission rates, so that the correlation plot is a test only of the transport and dispersion model. For d, we use the log transform of the concentration

$$d = \ln C_{pred} - \ln C_{obs} = \ln\left(\frac{C_{pred}}{C_{obs}}\right) \qquad (42)$$

because this is close to a normal distribution for the PDF model (see Hanna et al. 1986; Weil et al. 1992). Ideally, C_{pred}/C_{obs} should be 1, or $d = 0$, on average.

Figure 9 shows the correlation between the observed and predicted C/Q for both datasets. Despite the significant scatter, the geometric mean (GM) and geometric standard deviation (GSD) of C_{pred}/C_{obs} are 0.89 and 2.0 for Kincaid, and 1.1 and 2.1 for Maryland; the GMs are close to the ideal value of 1. In addition, the fraction r^2 of the variance explained by the model is 0.38 and 0.42 for Kincaid and Maryland, respectively, where r is the correlation coefficient between $\ln(C_{obs}/Q)$ and $\ln(C_{pred}/Q)$. As shown in Table 3, the above statistics are comparable to or perhaps slightly better than those attained with the earlier model of Weil et al. (1986); in Table 3, the r^2 is for $\ln C_{obs}$ versus $\ln C_{pred}$ (without the normalization by Q).

The large scatter in Fig. 9 arises from 1) the natural variability in concentration due to the stochastic nature of dispersion, 2) uncertainties or errors in the model input variables, 3) errors in the model physics, and 4) errors in the concentration measurements (Fox 1984;

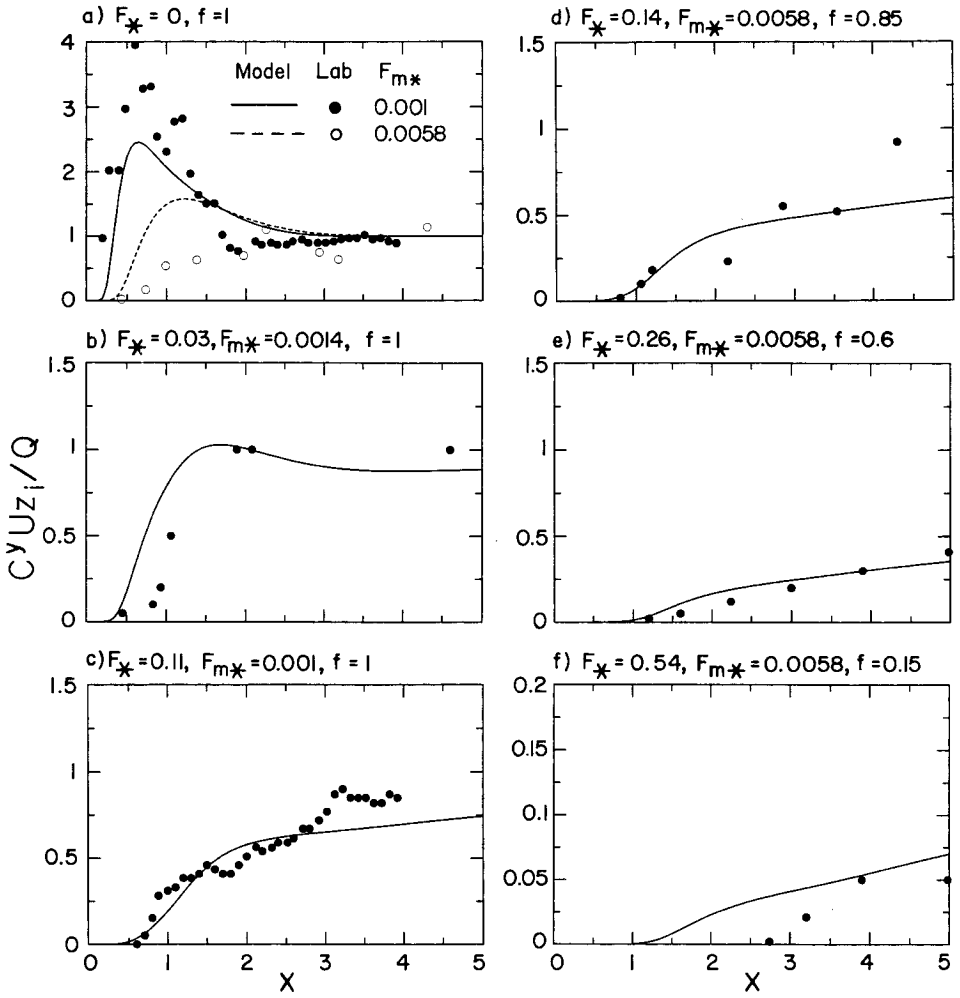

FIG. 7. Dimensionless crosswind-integrated concentration at the surface as a function of the dimensionless downwind distance for six values of F_*. Laboratory data are from (a) Deardorff and Willis (1984; F_{m*} = 0.001) and Willis and Deardorff (1987; F_{m*} = 0.0058), (b) Deardorff and Willis (1988), (c) Deardorff and Willis (1984), and (d)–(f) Willis and Deardorff (1987); h_s/z_i = 0.13 or 0.16.

Venkatram 1982; Weil et al. 1992). Here, we believe that the primary causes of the scatter are the natural variability and model input uncertainties, but there is also a contribution from model physics errors, as discussed below.

To put the above results in perspective, we show a similar plot (Fig. 10) for the Environmental Protection Agency (EPA) CRSTER model (EPA 1977), which is a standard Gaussian plume model based on the Pasquill–Gifford dispersion parameters; the plot is from an earlier analysis in which the concentrations were not normalized by Q (Weil et al. 1986). The CRSTER treatment of elevated sources is essentially the same as in the more widely used Industrial Source Complex (ISC) model (EPA 1987). As can be seen, the scatter in Fig. 10 is considerably greater than that in Fig. 9 and a significant number of zero predictions occur. The zeroes are associated with nonzero, and sometimes large, observed GLCs and are caused by predictions of complete plume penetration of the elevated inversion with no plume–ground contact. For the nonzero predictions, the GM, GSD, and r^2 are 1.0, 4.1, and 0.02, respectively; the larger GSD and smaller r^2 than in Fig. 9 are consistent with the greater scatter in Fig. 10.

The residuals from Fig. 9 are divided into groups or bins of points with respect to the variables F_*, U/w_*, and X, with the same bin widths as used in earlier work (Hanna et al. 1986; Weil et al. 1992). For each group, the GM, GSD, and uncertainty in the GM of $C_{\text{pred}}/C_{\text{obs}}$ are determined; the uncertainty is estimated from the 95% confidence limits of a lognormal distribution using the GSD and number of points in each group. In the following, we discuss the trends of the GMs with the variables.

Figure 11 shows the residual plot for F_*, where the horizontal line corresponds to a perfect model with the GM = 1 for all F_* bins, which are denoted by the vertical bars along the horizontal line. For each bin, the

TABLE 2. Model evaluation results based on comparisons between predicted and observed ground-level concentrations.

Model parameters	Plant	Cases	N[a]	GM[b]	GSD[c]	r^{2}[d]	Factor of 2 (%)[e]	Number of zero predictions[f]
$a_e = 0.1$, $R = 2$	Kincaid	All	302	0.89	2.0	0.38	71	0
$\partial\Theta_i/\partial z = 0.005$°C m^{-1}		$F_* \geq 0.1$	74	1.1	2.1		66	0
		$F_* < 0.1$	228	0.84	1.9		72	0
	Maryland	All	144	1.1	2.1	0.42	69	1
		$F_* \geq 0.1$	24	1.0	2.2		71	1
		$F_* < 0.1$	120	1.1	2.1		68	0
$a_e = 0.05$, $R = 2$	Kincaid	All	302	0.86	2.0	0.37	69	0
$\partial\Theta_i/\partial z = 0.005$°C m^{-1}	Maryland	All	144	1.1	2.1	0.42	69	1
$a_e = 0.15$, $R = 2$	Kincaid	All	302	0.90	2.0	0.38	71	0
$\partial\Theta_i/\partial z = 0.005$°C m^{-1}	Maryland	All	144	1.1	2.1	0.43	67	1
$a_e = 0.1$, $R = 1$	Kincaid	All	302	0.92	2.0	0.40	72	0
$\partial\Theta_i/\partial z = 0.005$°C m^{-1}	Maryland	All	144	1.2	2.2	0.39	67	1
$a_e = 0.1$, $R = 2$	Kincaid	All	302	0.91	2.1	0.34	69	0
$\partial\Theta_i/\partial z = 0.01$°C m^{-1}	Maryland	All	144	1.1	2.1	0.42	67	1
$a_e = 0.1$, $R = 2$	Kincaid	All	302	0.90	2.2	0.30	68	1
$\partial\Theta_i/\partial z = 0.02$°C m^{-1}	Maryland	All	144	1.1	2.1	0.42	67	1

[a] N—number of comparisons exclusive of zero predictions.
[b] GM—geometric mean of C_{pred}/C_{obs}.
[c] GSD—geometric standard deviation of C_{pred}/C_{obs}.
[d] r^2—variance between $\ln(C_{obs}/Q)$ and $\ln(C_{pred}/Q)$.
[e] Predictions within a factor of 2 of the observations.
[f] Zero predictions not included in GM, GSD, and r^2 statistics.

GM of C_{pred}/C_{obs} is denoted by the squares, and the GM uncertainty and GSD are represented by the innermost and outermost horizontal bars, respectively, on the vertical lines through the squares.

Considering both datasets, we see that the residual dependence on F_* is mixed. For Kincaid (Fig. 11a), the residuals exhibit a trend showing 1) a slight model underprediction for $F_* < 0.1$ (GM = 0.84), 2) a modest overprediction for $0.1 \leq F_* < 0.4$ (GM = 1.28), and 3) a clear underprediction for $F_* > 0.4$ (GM = 0.44). We suspect that the difference between groups 1 and 2 above is due to deficiencies in (a) the indirect source model, which depends on F_*, and (b) the penetrated plume model, which makes some GLC contributions in group 2, but none in group 1. For $F_* > 0.4$, the underprediction is due solely to the penetrated plume model since the predicted $f = 0$ for all 14 cases in this group. The cases occurred in the morning, with low z_i values (200 m $< z_i <$ 300 m), generally light winds ($U < 3$ m s^{-1}), and a small w_* (1–1.4 m s^{-1}). The indirect source and penetrated plume models are discussed further in section 5.

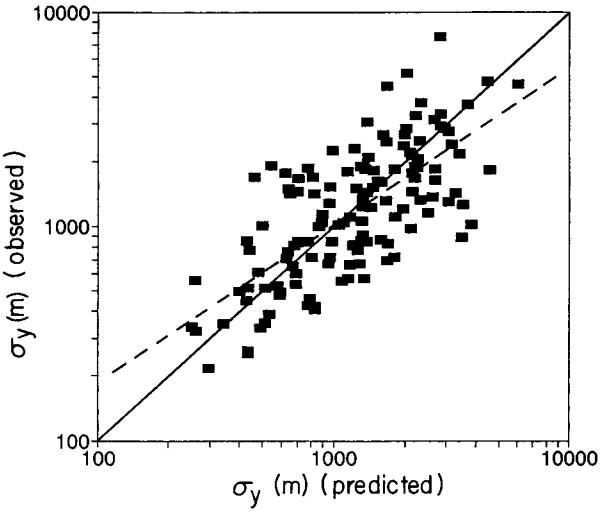

FIG. 8. Comparison between observed and predicted lateral dispersion parameter of buoyant plumes at Maryland power plants. Solid line corresponds to equal values of observations and predictions; dashed line is a least squares fit of $\ln\sigma_{yobs}$ to $\ln\sigma_{ypred}$.

In contrast to the Kincaid results, the C_{pred}/C_{obs} ratio for the Maryland plants exhibits no statistically significant trend with F_* (Fig. 11b). For the Maryland data and $F_* \geq 0.1$, there are probably too few observations (24) to draw firm conclusions about the performance of the penetrated plume model.

Figure 12 shows the residuals as functions of U/w_*. The Kincaid results exhibit a weak trend, with the GM differing statistically from 1 in the interval $1.2 < U/w_* \leq 5$. The slight overprediction for $U/w_* \leq 1.2$ is caused by the high F_* cases; if the latter are removed, the GM falls from 1.2 to 1.0 in this interval.

Of the variables studied, the Maryland residuals exhibit their most significant variation with U/w_* (Fig. 12b). Most of this is caused by GLC observations obtained on the downwind side of wide (~1–10 km) rivers

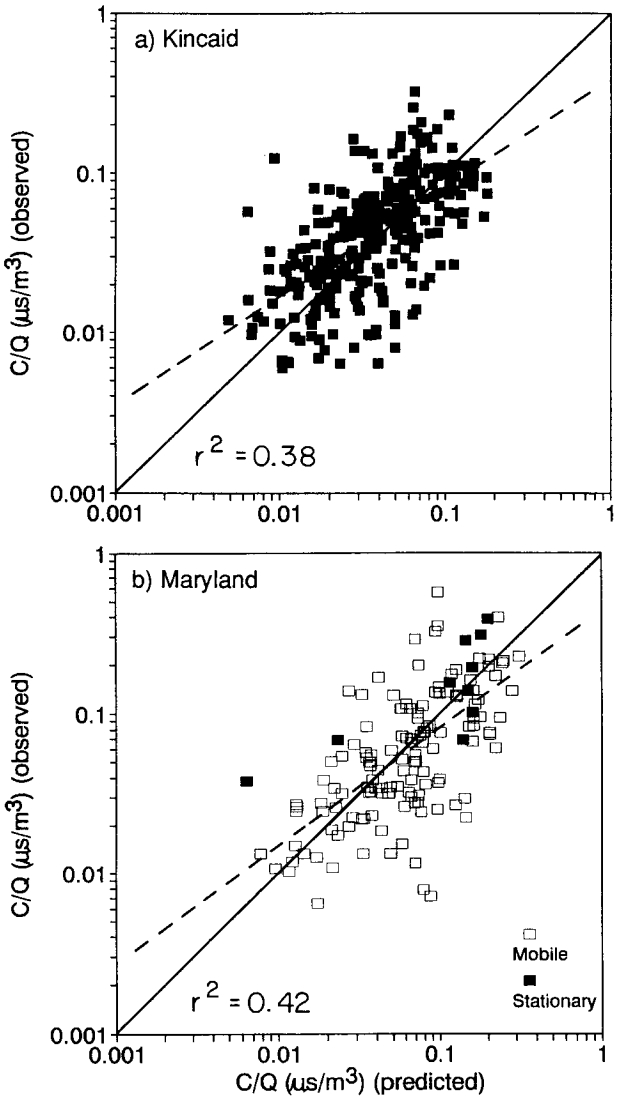

FIG. 9. Observed versus predicted ground-level concentrations for the PDF model at (a) Kincaid power plant for SF_6 concentrations and (b) Maryland power plants for SO_2 concentrations. Solid line corresponds to equal values of observations and predictions; dashed line is a least squares fit of $\ln(C/Q)_{obs}$ to $\ln(C/Q)_{pred}$.

bordering the Chalk Point and Morgantown plants (Weil and Corio 1985). We suspect that reduced heat fluxes and turbulence levels due to the cooler water (than land) surface would induce local circulations and temporarily diminish dispersion on the downwind side of the rivers. Removal of the 25 near-river cases results in a residual, or GM behavior, given by the open circles (Fig. 12b), which show somewhat less of a trend.

Figure 13 shows the residuals as a function of X, and again, there are mixed results for the two datasets. For Kincaid, we believe that the underestimated GLCs in the interval $2 \leq X < 5$ are caused by an overestimated vertical dispersion, particularly for wind speeds in the range $2 \leq U/w_* < 5$ (see Fig. 12a). A good example of the difference between the modeled and observed behavior is shown in Fig. 14a, where the dimensionless GLC CUz_i^2/Q is plotted versus X for a 4-h period on 1 day. The lower observed maximum GLC and the greater distance to it than predicted (lines) imply an overestimated vertical dispersion. Figure 14b shows a similar, but less extreme, example of an underprediction bias in the $2 \leq X < 5$ interval. A modification of the vertical dispersion formulation to correct the above bias is discussed in section 5b.

For the Maryland plants (Fig. 13b), the residuals are statistically unbiased and independent of X. The greatest departure of the GM from 1 occurs for $X \leq 1$ and is due to the near-river observations at the Chalk Point and Morgantown plants. For $X \leq 1$, the GM of C_{pred}/C_{obs} is 2.0, 5.0, and 0.82 for Chalk Point, Morgantown, and Dickerson, respectively.

Overall, the above results show that the GMs of C_{pred}/C_{obs} in the various intervals range from about 0.8 to 1.25, which is considered good. Some exceptions to this and trends in the GMs were discussed in terms of model deficiencies and physical processes omitted. These include 1) limitations in the indirect source and penetrated plume models, 2) overestimated vertical dispersion for moderate winds, and 3) reduced heat fluxes and dispersion on the downwind side of wide rivers bordering two power plants.

Table 2 presents the overall statistical results for the above ''base case'' model, with $a_e = 0.1$, $R = 2$, and $\partial\Theta_i/\partial z = 0.005°\text{C m}^{-1}$; note that about 70% of the predictions are within a factor of 2 of the observations. The results for other parameter values do not vary significantly from these base case results, which suggests that the model is fairly robust for the parameter ranges investigated.

As a final demonstration of model performance, we present quantile–quantile plots in Fig. 15 for the Kincaid and Maryland data. The results are obtained by ranking the C_{pred} and C_{obs} values from the lowest to highest and plotting the concentrations corresponding to the same rank in each distribution. This is not a rigorous test of model performance, but it is a useful comparison for air quality applications (e.g., Cimorelli et al. 1996). As can be seen, the results fall close to the 1:1 line, indicating good agreement between the ranked distributions. The maximum deviation from this line occurs at the high end of the distribution, where $C_{pred} \sim 0.5C_{obs}$. This deviation may be explained by the neglect of stochastic variability in the model and requires further investigation.

5. Discussion

In the following, we discuss several model features affecting the GLCs: 1) the w PDF parameterization, 2) the vertical dispersion and the effect of a finite T_{Lz}, and 3) the indirect source and penetrated plume models.

TABLE 3. Evaluation results for current and Weil et al. (1986) models based on comparisons between predicted and observed ground-level concentrations.

Model version	Plant	Cases	GM[a]	GSD[b]	r^{2}[c]	Factor of 2 (%)[d]
Current	Kincaid	All	0.89	2.0	0.38	71
		$F_* \geq 0.1$	1.1	2.1	0.32	66
		$F_* < 0.1$	0.84	1.9	0.34	72
Weil et al. (1986)	Kincaid	All	1.1	2.1	0.34	68
		$F_* \geq 0.1$	1.3	2.3	0.30	53
		$F_* < 0.1$	1.0	2.0	0.32	74
Current	Maryland	All	1.1	2.1	0.50	69
		$F_* \geq 0.1$	1.0	2.2	0.51	71
		$F_* < 0.1$	1.1	2.1	0.38	68
Weil et al. (1986)	Maryland	All	1.3	2.2	0.50	68
		$F_* \geq 0.1$	1.0	3.0	0.43	56
		$F_* < 0.1$	1.4	2.0	0.45	70

[a] GM—geometric mean of C_{pred}/C_{obs}.
[b] GSD—geometric standard deviation of C_{pred}/C_{obs}.
[c] r^2—variance between $\ln(C_{obs})$ and $\ln(C_{pred})$.
[d] Predictions within a factor of 2 of the observations.

a. The w PDF parameterization

The existing p_w is based on the first three moments of w—$\overline{w}$, σ_w^2, and $\overline{w^3}$—and the assumption that $\sigma_{w1}/\overline{w_1} = |\sigma_{w2}/\overline{w_2}| = R$. This is one parameterization, and alternatives should be considered. For example, Weil (1988) used the bi-Gaussian form [Eq. (7)] with an assumed $\lambda_1 = 0.4$ and $\lambda_2 = 0.6$, but empirically obtained the σ_{wj} and $\overline{w_j}$ from a fit of the modeled surface CWIC distribution to laboratory data for passive releases. Using his σ_{wj} and $\overline{w_j}$, we find $\sigma_{w1}/\overline{w_1} = 1.2$ and $\sigma_{w2}/|\overline{w_2}| = 0.74$. The key point is that the $\sigma_{wj}/|\overline{w_j}|$ ratios are unequal, in contrast to our earlier assumption.

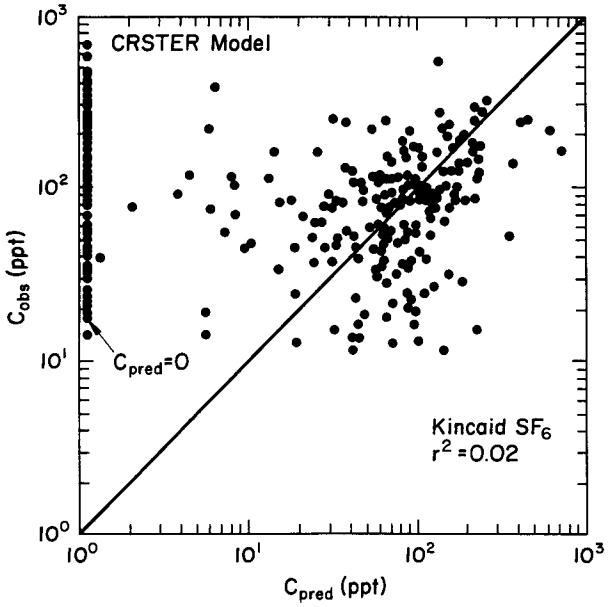

FIG. 10. Observed versus predicted ground-level SF_6 concentrations for the CRSTER model at the Kincaid power plant; diagonal line corresponds to $C_{obs} = C_{pred}$.

In a study of the bi-Gaussian PDF, Du et al. (1994) added the fourth moment of w to the input variables and specified $\lambda_1 = 0.4$ and $\lambda_2 = 0.6$ for strong convection. Using their σ_{wj} and $\overline{w_j}$ expressions, we find $\sigma_{w1}/\overline{w_1} = 2.89$ and $\sigma_{w2}/\overline{w_2} = 2.08$ for $S = 0.1$, $\sigma_{w1}/\overline{w_1} = 1.07$ and $\sigma_{w2}/\overline{w_2} = 1.03$ for $S = 0.6$, and $\sigma_{w1}/\overline{w_1} = 0.93$ and $\sigma_{w2}/\overline{w_2} = 0.73$ for $S = 0.8$. Their ratios increase as $S \rightarrow 0$, as would be expected for a distribution approximating a Gaussian PDF in that limit, and for $S = 0.8$, they are close to those obtained from Weil's (1988) empirical fit. Thus, the addition of $\overline{w^4}$ to the input variables may improve the p_w parameterization, and perhaps the agreement between predicted and observed GLCs.

The Du et al. (1994) approach for estimating the p_w parameters should be pursued in the future. This approach could be improved further by parameterizing the λ_1 and λ_2 as functions of S such that $\lambda_1, \lambda_2 \rightarrow 0.5$ as $S \rightarrow 0$. However, one must consider the uncertainty in estimates or measurements of $\overline{w^4}$ and the associated uncertainty in C_{pred} before implementing this approach in a practical model.

b. Vertical dispersion

The results of section 4b for the Kincaid plant suggest an apparent overestimation of the vertical dispersion during moderate winds. This may be partially caused by the infinite, rather than the finite, T_{Lz} assumed for the CBL.

Here, we demonstrate the effect of a finite T_{Lz} on vertical dispersion and the distance x_m to the maximum GLC. We first consider a Gaussian plume model for a passive release, with the GLC along the plume centerline given by

$$C(x, 0, 0) = \frac{Q}{\pi U \sigma_y \sigma_z} \exp\left(-\frac{h_s^2}{2\sigma_z^2}\right). \qquad (43)$$

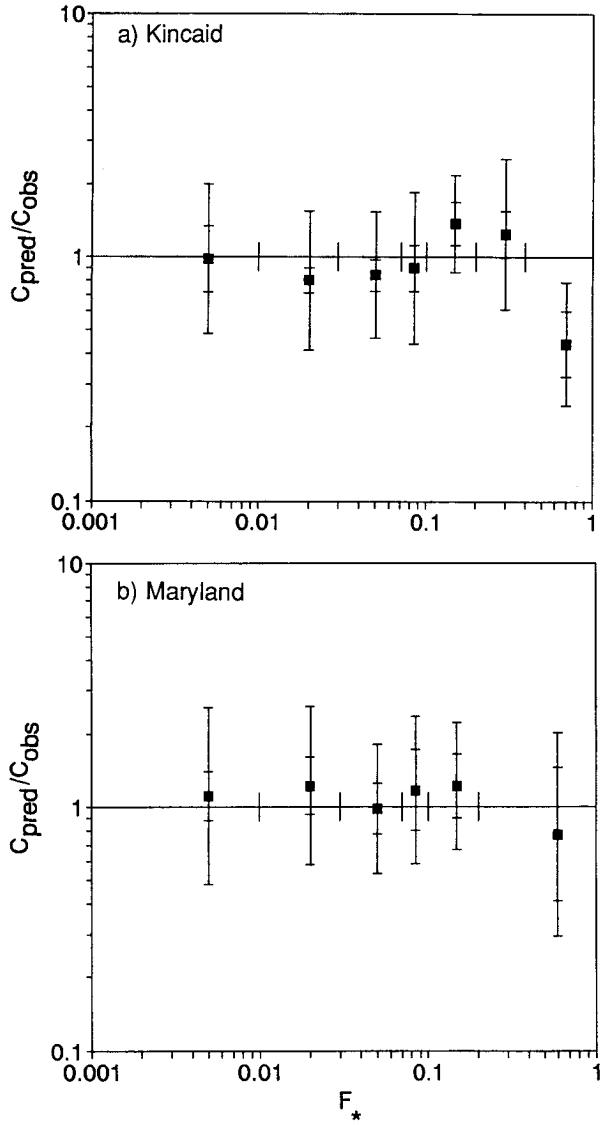

FIG. 11. Geometric mean (points) of predicted-to-observed ground-level concentration as a function of the dimensionless buoyancy flux for the PDF model. Innermost and outermost horizontal bars denote the uncertainty in the GM and the geometric standard deviation, respectively.

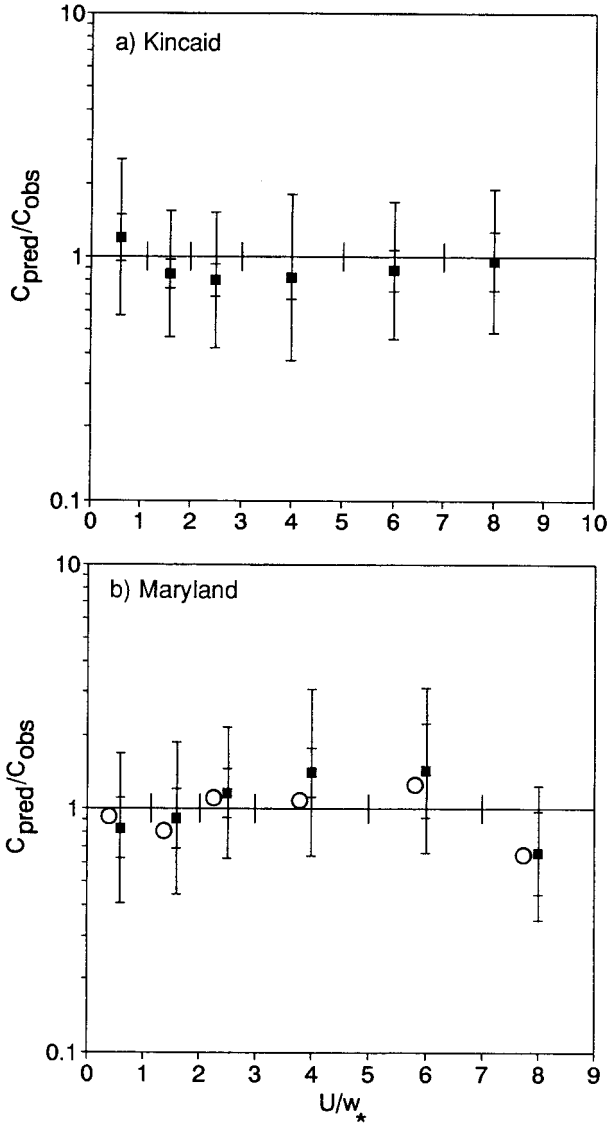

FIG. 12. Geometric mean (points) of predicted-to-observed ground-level concentration as a function of U/w_* for the PDF model. Innermost and outermost horizontal bars denote the uncertainty in the GM and the geometric standard deviation, respectively. Open circles in (b) denote GMs without near-river cases at the Chalk Point and Morgantown plants.

The σ_z is parameterized by $\sigma_z = \sigma_w t(1 + 0.5t/T_{Lz})^{-1/2}$ and similarly for σ_y, but with σ_w replaced by σ_v; we assume $T_{Ly} = T_{Lz}$. These parameterizations satisfy the short- and long-time limits of Taylor's (1921) theory.

The travel time t_m corresponding to the x_m is found by taking $\partial C/\partial t$ in Eq. (43) and setting it equal to zero. The t_m is attained when $2\sigma_z^2 = h_s^2$ and is

$$t_m = \frac{h_s^2}{8\sigma_w^2 T_{Lz}}\left[1 + \left(1 + \frac{32\sigma_w^2 T_{Lz}^2}{h_s^2}\right)^{1/2}\right], \qquad (44)$$

with $x_m = Ut_m$. Assuming that $\sigma_w^2 = 0.31w_*^2$ and $T_{Lz} = 0.7z_i/w_*$, we find the dimensionless distance X_m corresponding to x_m to be

$$X_m = \frac{w_* x_m}{Uz_i} = 0.58h_s^{*2}\left[1 + \left(1 + \frac{4.9}{h_s^{*2}}\right)^{1/2}\right], \qquad (45)$$

where $h_s^* = h_s/z_i$. In the limit of an infinite T_{Lz}, the t_m and X_m are given by $t_{m\infty} = h_s(\sqrt{2}\sigma_w)^{-1}$ and $X_{m\infty} = 1.26h_s^*$, assuming $\sigma_w = 0.56w_*$.

We now consider the variation of the ratio $X_m/X_{m\infty}$ with source height. For $h_s^* = 0.1$, 0.25, 0.5, and 1, the $X_m = 0.13$, 0.36, 0.8, and 2.0, and the $X_m/X_{m\infty} = 1.02$, 1.13,1.26, and 1.56. As expected, the ratio increases with h_s^* because of the greater time required for the plume to reach the surface from a more elevated source.

With the greater time, the growth rate is reduced since t is further into the long-time or $t^{1/2}$ regime of spread. Qualitatively, we expect the $X_m/X_{m\infty}$ ratio to increase further with the addition of plume buoyancy because of the greater effective source height.

In the following, a simple approach is outlined for including the T_{Lz} effect for buoyant plumes and a skewed p_w. We reconsider the trajectory expression [Eq. (5)] and assume that the random vertical velocity decays from its initial value w over time according to $w/f_L(t)$, where $f_L(t)$ is taken here to be $(1 + 0.5t/T_{Lz})^{1/2}$. With $t = x/U$, the new trajectory equation is

$$z_p = h_s + \Delta h + \frac{wt}{f_L(t)}, \tag{46}$$

and the $w(z_p; t)$ found by rearranging the above is

$$w = (z_p - h_s - \Delta h)\frac{f_L(t)}{t}. \tag{47}$$

From Eq. (47), we have $|dw/dz_p| = f_L(t)/t$.

The above w and dw/dz_p can be substituted into Eq. (4) to obtain the p_z. Upon doing this, replacing t by x/U, and using Eq. (3), we obtain a $C^y(x, z)$ expression identical to Eq. (9), but with σ_{zj} and Ψ_j given by

$$\sigma_{zj} = \frac{\sigma_{wj}x/U}{(1 + 0.5x/UT_{Lz})^{1/2}}$$

and

$$\Psi_j = h_s + \Delta h + \frac{\overline{w_j}x/U}{(1 + 0.5x/UT_{Lz})^{1/2}}, \tag{48}$$

with $j = 1$ or 2. For a Gaussian p_w and $\Delta h = 0$, this approach reproduces Eq. (43) for the GLC.

As Eq. (48) shows, the vertical dispersion (σ_{zj}) at a given x becomes smaller as T_{Lz} is reduced, and thus x_m becomes larger. The T_{Lz} is expected to decrease with decreasing $z_i/|L|$ because of the increased turbulence dissipation rate ε and the decreased turbulence length scale l, especially within the surface layer. The behavior of ε is shown by the observations of Guillemet et al. (1983) and that of l by the large-eddy simulations (LES) of Mason (1992). In addition, Mason's dispersion simulations using a Lagrangian model and LES fields show that a systematic reduction in vertical dispersion occurs with a decreasing w_*/u_* or $z_i/|L|$ and increasing wind speed. These findings are consistent with the inferred overestimation of the vertical dispersion at the Kincaid plant (Figs. 12a and 13) for moderate winds.

The approach outlined above [Eqs. (46)–(48)] will be pursued in the future for a skewed p_w, with comparisons made between predicted and observed GLCs.

c. Indirect source and penetrated plume models

The Kincaid residual analysis for F_* (Fig. 11a) suggests that the indirect source model needs further development. There are two aspects that could be improved. The first is the inclusion of the finite T_{Lz}, which would shift the axial GLC distribution farther downwind and reduce the GLC magnitude; these changes should be more pronounced for the high-F_* cases ($0.1 \leq F_* < 0.4$), where model overestimation is a problem. The second is a better Δh_i model.

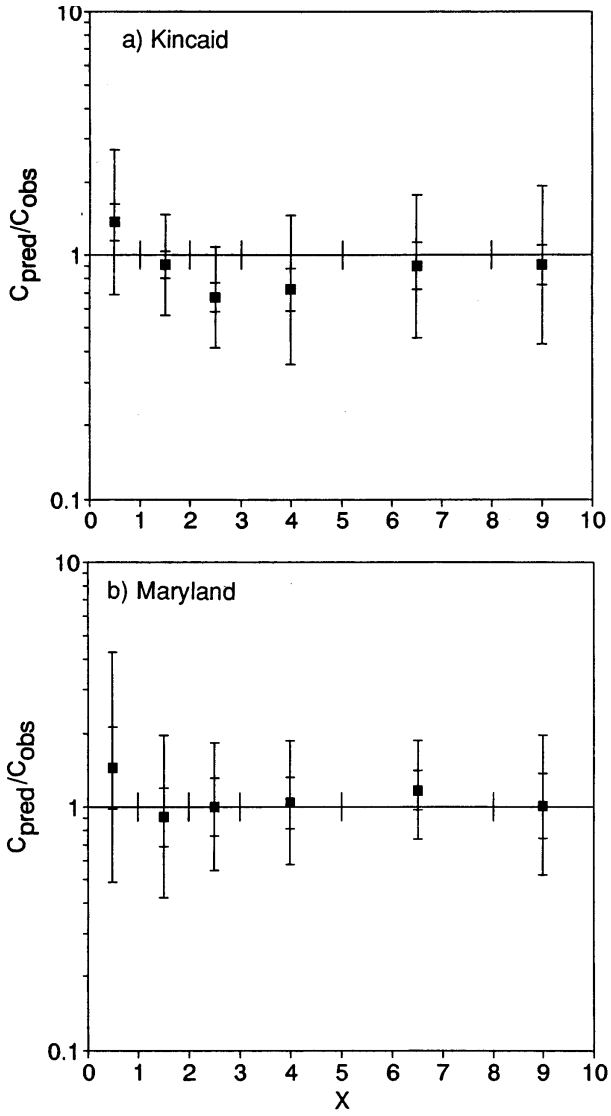

FIG. 13. Geometric mean (points) of predicted-to-observed ground-level concentration as a function of the dimensionless downwind distance for the PDF model. Innermost and outermost horizontal bars denote the uncertainty in the GM and the geometric standard deviation, respectively.

While the above improvements are worth pursuing, we must recognize the limitations of the indirect source formulation: Δh_i is somewhat of a ''fictitious'' plume rise, and the r_z ($\propto x^{4/3}$) far downwind (appendix C) probably exhibits too rapid a growth rate. Thus, we should consider alternative treatments for the indirect source, such as a distributed source with x as originally adopted by Hanna et al. (1986). This could be expanded to in-

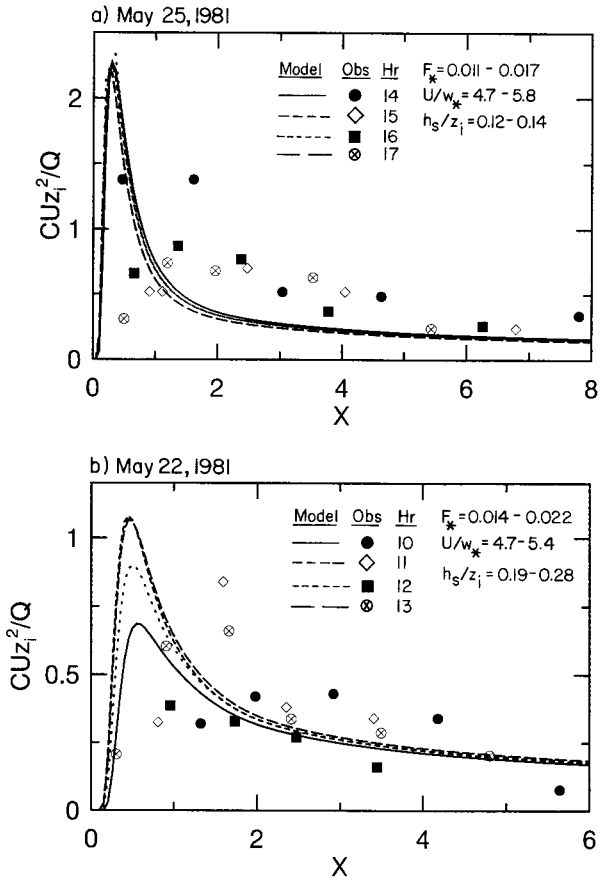

FIG. 14. Dimensionless ground-level SF_6 concentration versus the dimensionless downwind distance as observed at the Kincaid power plant and predicted by the PDF model.

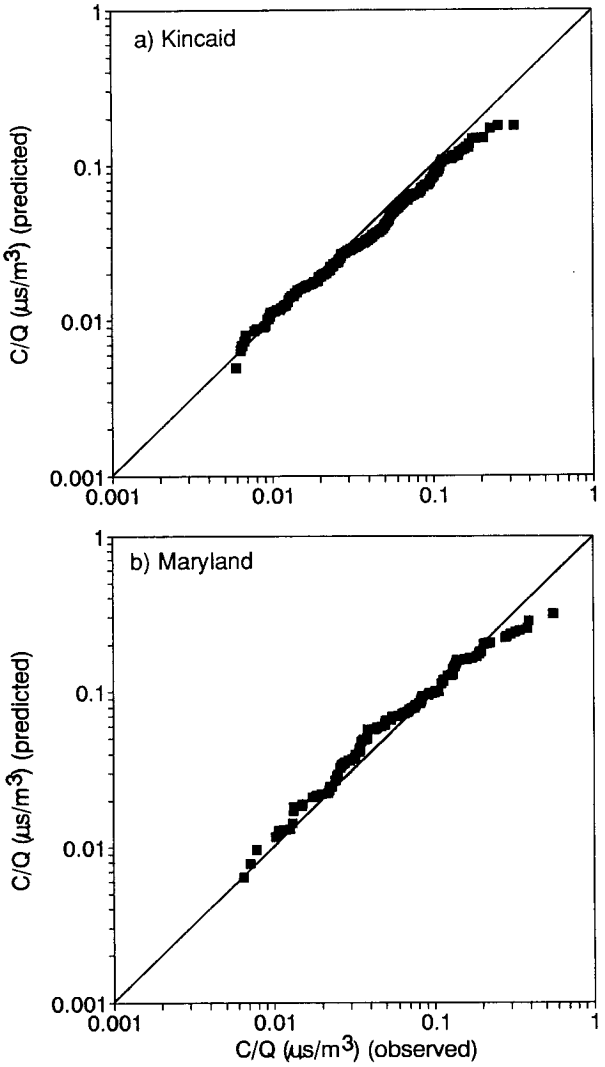

FIG. 15. Quantile–quantile plots of predicted versus observed ground-level concentration for the Kincaid and Maryland datasets.

clude an increasing $\tilde{z}_i$ with t over the averaging period, which is important in the morning, when many high-F_* cases occur. Systematic experiments in a convection tank would be helpful for further development efforts.

The penetrated plume model is an ad hoc approach that only roughly accounts for the CBL growth and fumigation. An important feature to add is the distributed nature of the source, which is included in other fumigation models (Deardorff and Willis 1982; Luhar and Sawford 1995; Misra 1980; Venkatram 1988). This aspect, as well as the time dependence of $\tilde{z}_i$, h_{es}, f, etc., should be incorporated into a more general formulation. Although such a formulation would be more complex, it should be pursued to determine whether it leads to better predictions.

6. Summary and conclusions

A PDF dispersion model has been presented for buoyant releases in the CBL, where the mean concentration field C is found from the particle position PDFs, p_y and p_z. The p_z is derived from the vertical velocity (w) PDF, which is generally skewed, whereas the p_y is assumed to be Gaussian. Three primary sources contribute to the modeled C field: 1) the direct or real source (at the stack), 2) the indirect source, and 3) the penetrated source. Image sources are included to satisfy the zero-flux conditions at $z = 0$, z_i. The indirect and penetrated source models are simple approaches for treating the plume interaction with the elevated inversion and lead to a continuous variation of C with the buoyancy flux.

Comparisons between modeled crosswind-integrated concentration fields (C^y) and convection tank data (Deardorff and Willis 1984, 1988; Willis and Deardorff 1987) showed fair to good agreement in the lower half of the CBL. Near the source, the predicted C^y contours exhibited an upward tilt due to the plume rise, with the tilt increasing with the buoyancy flux. However, the predicted contour behavior near the CBL top differed from the measurements due to the assumed quasi re-

flection at $z = z_i$; improvement of this aspect is a problem for future work. Overall, the predicted C^y profiles at the surface were in agreement with the data over a wide range of the buoyancy flux and showed a progressive reduction in the C^y with increasing F_*.

The model was also evaluated with GLCs measured near several Maryland power plants and the Kincaid power plant. Correlation plots of C/Q for each dataset exhibited considerable scatter, but the r^2 between predicted and observed $\ln(C/Q)$ values was approximately 0.4 for both sets, thus demonstrating an overall consistency of model performance. In addition, the statistics of $C_{\text{pred}}/C_{\text{obs}}$ were good, with a GM near 1 and a GSD of about 2. These results were similar to those obtained with the Weil et al. (1986) model (Table 3). Thus, in addition to maintaining a continuous variation of C with F_*, a problem with earlier PDF models, the current model yields performance results comparable to those models.

The model performance was diagnosed further using residual plots to detect model trends with the input variables; the variables included the buoyancy flux, wind speed, and downwind distance. In general, the GMs of $C_{\text{pred}}/C_{\text{obs}}$ for grouped data ranged from 0.8 to 1.25, which is considered good. Some exceptions to this and trends in the GMs were found, suggesting some model limitations. The latter included 1) limitations in the indirect source and penetrated plume models, 2) overestimated vertical dispersion during moderate winds, and 3) reduced heat fluxes and dispersion on the downwind side of wide rivers bordering two power plants.

In summary, the PDF model is an approach that includes state-of-the-art knowledge of CBL turbulence and dispersion in a simple framework. The overall model performance is good. Future development efforts should focus on 1) improving the indirect source and penetrated plume models, and 2) incorporating a finite Lagrangian timescale (T_{Lz}) into the model to correct the overestimated vertical dispersion during moderate winds (section 5b).

Acknowledgments. We wish to thank S. White and J. Walker for their assistance with the data analysis and for preparing the figures, K. Davis and T. Horst for comments on an earlier draft of this paper, and two anonymous reviewers for their comments. We also are grateful to G. A. Briggs and members of the American Meteorological Society–Environmental Protection Agency Regulatory Model Improvement Committee—A. Cimorelli, R. Lee, R. Paine, S. Perry, A. Venkatram, and R. Wilson—for helpful discussions and comments during the course of this work. This research was supported by the Maryland Department of Natural Resources and by the U.S. Environmental Protection Agency under Grant R-823419-01-0.

APPENDIX A

Parameters Defining the *w* PDF

The parameters of $p_w(w)$ in Eq. (7) are obtained by equating the zeroth through third moments of that distribution,

$$\overline{w^n} = \int_{-\infty}^{\infty} w^n p_w(w)\, dw \tag{A1}$$

($n = 0$–3), with those specified: $\overline{w^0} = \lambda_1 + \lambda_2 = 1$, $\overline{w} = 0$, σ_w^2 [Eq. (8a)], and $\overline{w^3} = S\sigma_w^3$. The equations are given in Baerentsen and Berkowicz (1984) and Weil (1990).

Defining $R = \sigma_{w1}/\overline{w_1} = -\sigma_{w2}/\overline{w_2}$, Weil (1990) found the solutions for $\overline{w_1}$ and $\overline{w_2}$ to be

$$\frac{\overline{w_1}}{\sigma_w} = \frac{\gamma_1 S}{2} + \frac{1}{2}\left(\gamma_1^2 S^2 + \frac{4}{\gamma_2}\right)^{1/2} \tag{A2}$$

and

$$\frac{\overline{w_2}}{\sigma_w} = \frac{\gamma_1 S}{2} - \frac{1}{2}\left(\gamma_1^2 S^2 + \frac{4}{\gamma_2}\right)^{1/2}, \tag{A3}$$

where

$$\gamma_1 = \frac{1 + R^2}{1 + 3R^2} \tag{A4}$$

and

$$\gamma_2 = 1 + R^2. \tag{A5}$$

In addition, he obtained

$$\lambda_1 = \frac{\overline{w_2}}{\overline{w_2} - \overline{w_1}} \tag{A6}$$

and

$$\lambda_2 = -\frac{\overline{w_1}}{\overline{w_2} - \overline{w_1}}, \tag{A7}$$

as found by Baerentsen and Berkowicz.

Thus, with σ_w^2, S, and R specified, the $\overline{w_j}$, σ_{wj}, and $\lambda_j (j = 1, 2)$ can be found.

APPENDIX B

Estimation of the Parameter α in the Energy Criterion

In the following, we apply the energy criterion of Eq. (19) to estimate the negative heat or buoyancy flux at the top of the CBL, which is assumed to be capped by a positive potential temperature jump $\Delta\Theta = \Theta_2 - \Theta_1$, where 2 and 1 denote conditions above and below the jump. Assuming small temperature and density ($\Delta\rho = \rho_1 - \rho_2$) jumps, the two are related by $\Delta\Theta/\Theta_a = \Delta\rho/\rho_a$. Using the last relationship, we rewrite Eq. (19) in the form

$$g\frac{\Delta\Theta}{\theta_a} = \alpha\frac{w^2}{2z_i}. \tag{B1}$$

Within the PDF model framework, we assume that negative vertical velocities above z_i transport warm air downward into the CBL to be mixed. We estimate a

negative buoyancy flux by multiplying Eq. (B1) by w and averaging over the negative velocities as

$$\frac{1}{f_d}\int_{-\infty}^{0} wg\frac{\Delta\Theta}{\Theta_a}p_w\,dw = \frac{1}{f_d}\int_{-\infty}^{0}\frac{\alpha}{2z_i}w^3p_w\,dw, \quad \text{(B2)}$$

where

$$f_d = \int_{-\infty}^{0} p_w\,dw. \quad \text{(B3)}$$

The left-hand side (lhs) of (B2) is the negative buoyancy flux at the inversion, $(g/\Theta_a)\overline{w\theta_i}$, which is generally assumed to be related to the surface buoyancy flux by

$$-\frac{g}{\Theta_a}\overline{w\theta_i} = 0.2\frac{g}{\Theta_a}\overline{w\theta_o} \quad \text{(B4)}$$

(see Moeng and Wyngaard 1989). Replacing the lhs of (B2) by the right-hand side of (B4), we have

$$0.2\frac{g}{\Theta_a}\overline{w\theta_o} = \frac{1}{f_d}\frac{\alpha}{2z_i}\int_{-\infty}^{0} w^3p_w\,dw. \quad \text{(B5)}$$

For simplicity in evaluating the above integral, we assume a Gaussian PDF, which leads to

$$0.2\frac{g}{\Theta_a}\overline{w\theta_o} = \frac{2\alpha}{\sqrt{2\pi}}\frac{\sigma_w^3}{z_i}. \quad \text{(B6)}$$

Using the definition of $w_* = (g\overline{w\theta_o}z_i/\Theta_a)^{1/3}$, we have

$$0.2w_*^3 = \frac{2\alpha}{\sqrt{2\pi}}\sigma_w^3. \quad \text{(B7)}$$

Evaluating (B7) with the convective limit of Eq. (8a) ($\sigma_w = 0.56w_*$), we find $\alpha = 1.4$.

APPENDIX C

Growth of Lofting Plumes

We consider a plume of elliptical cross section trapped at the CBL top and unable to penetrate the elevated inversion. The ellipse has half-widths r_y and r_z in the lateral and vertical directions (see Fig. 2c) and a uniform density defect, $\rho - \rho_a = -\Delta\rho$, relative to the density in the CBL. In line with Briggs (1985), we assume that the lateral dispersion is enhanced and the vertical dispersion is constant or diminished somewhat initially. The plume is assumed to behave as a stable density interface at the CBL top with entrainment taking place on the bottom half of the plume perimeter; this is akin to entrainment across the density or temperature jump in the environment at $z = z_i$. With the elliptical cross section, the cross sectional area is $\pi r_y r_z$ and the perimeter is approximated by $\pi(r_y + r_z)$.

Assuming that entrainment takes place only along the lower half of the plume, we use an entrainment assumption in a conservation expression for plume mass or volume, which yields

$$\frac{d}{dx}(Ur_yr_z) = \frac{w_e}{2}(r_y + r_z), \quad \text{(C1)}$$

where w_e is an entrainment velocity (Weil 1991). This is analogous to the conservation expression for a circular plume. For the elliptical plume with zero penetration of the inversion, the buoyancy flux F is conserved so that

$$F = F_b = Ur_yr_zg\frac{\Delta\rho}{\rho_a}. \quad \text{(C2)}$$

In line with entrainment models for turbulent mixed layers (e.g., Turner 1979; Deardorff and Willis 1985), we assume that

$$w_e = a_e\frac{w_*}{\mathrm{Ri}^{\mu}}, \quad \text{(C3)}$$

where Ri is a Richardson number based on the plume density defect and r_z:

$$\mathrm{Ri} = \frac{g\Delta\rho}{\rho_a}\frac{r_z}{w_*^2}. \quad \text{(C4)}$$

Using Eq. (C2), the Ri can be written as

$$\mathrm{Ri} = \frac{F_b}{Uw_*^2r_y}. \quad \text{(C5)}$$

Equation (C3) is chosen as a simple form for w_e that results in an analytical expression for the product r_yr_z. The exponent μ in Eq. (C3) is taken as 1/2 based on the entrainment velocity correlation with Ri from Deardorff and Willis (1985, their Fig. 20), where their Ri is defined using interfacial length and velocity scales.

Substituting Eqs. (C3) and (C5) into Eq. (C1), we have

$$\frac{d}{dx}(r_yr_z) = \frac{a_ew_*^2}{2}\left(\frac{r_y}{F_bU}\right)^{1/2}(r_y + r_z). \quad \text{(C6)}$$

To complete the model, we assume that 1) the half-width $r_y = \sqrt{2}\sigma_y$ (see Briggs 1975; Csanady 1973), 2) σ_y is given by Briggs's (1985) expression for lofting plumes $\sigma_y = 1.6F_b^{1/3}x^{2/3}/U$, and 3) $r_z \ll r_y$ far downstream. As a result of the last assumption, we have

$$\frac{d}{dx}(r_yr_z) = \frac{a_ew_*^2}{2(F_bU)^{1/2}}r_y^{3/2}. \quad \text{(C7)}$$

Substituting the expression for r_y into the above, we can integrate Eq. (C7) to obtain

$$r_yr_z = r_i^2 + \frac{a_e\alpha_y^{3/2}w_*^2}{4U^2}(x^2 - x_i^2), \quad \text{(C8)}$$

where r_i is the plume radius when the rising plume reaches the inversion, x_i is the distance where this occurs, and $\alpha_y = 1.6\sqrt{2} = 2.3$. In the main text and model, we ignore the x_i in (C8) since our interest is primarily

for $x \gg x_i$. The a_e is found to be 0.1 based on comparisons with laboratory data.

Far downstream, where r_i^2 and x_i^2 can be neglected in Eq. (C8), we have

$$r_z \simeq \frac{a_e \alpha_y^{3/2} w_*^2 x^2}{4U^2 r_y}. \tag{C9}$$

Substituting the r_y expression and the value of α_y into the above, we find

$$r_z \simeq 0.38 a_e \frac{w_*^2 x^{4/3}}{F_b^{1/3} U}. \tag{C10}$$

REFERENCES

Baerentsen, J. H., and R. Berkowicz, 1984: Monte Carlo simulation of plume dispersion in the convective boundary layer. *Atmos. Environ.*, **18,** 701–712.

Bowne, N. E., R. J. Londergan, D. R. Murray, and H. S. Borenstein, 1983: Overview, results and conclusions for the EPRI plume model validation and development project: Plains site. Electric Power Research Institute Rep. EA-3074, Electric Power Research Institute, Palo Alto, CA, 205 pp.

Briggs, G. A., 1975: Plume rise predictions. *Lectures on Air Pollution and Environmental Impact Analyses,* D. A. Haugen, Ed., Amer. Meteor. Soc., 59–111.

——, 1984: Plume rise and buoyancy effects. *Atmospheric Science and Power Production,* D. Randerson, Ed., U.S. Department of Energy.

——, 1985: Analytical parameterizations of diffusion: The convective boundary layer. *J. Climate Appl. Meteor.*, **24,** 1167–1186.

Brownlee, K. A., 1965: *Statistical Theory and Methodology.* Wiley and Sons, 550 pp.

Businger, J. A., 1973: Turbulent transfer in the atmospheric surface layer. *Workshop on Micrometeorology,* D. A. Haugen, Ed., Amer. Meteor. Soc., 67–100.

Carson, D. J., 1973: The development of a dry inversion-capped convectively unstable boundary layer. *Quart. J. Roy. Meteor. Soc.*, **99,** 450–467.

Chatwin, P. C., D. M. Lewis, and P. J. Sullivan, 1995: Turbulent dispersion and the beta distribution. *Environmetrics*, **6,** 395–402.

Cimorelli, A. J., S. G. Perry, R. F. Lee, R. J. Paine, A. Venkatram, J. C. Weil, and R. B. Wilson, 1996: Current progress in the AERMIC model development program. *Proc. 89th Annual Meeting and Exhibition of the Air and Waste Management Association,* Pittsburgh, PA, Air Waste Manage. Assoc.

Csanady, G. T., 1973: *Turbulent Diffusion in the Environment.* Reidel, 248 pp.

Deardorff, J. W., and G. E. Willis, 1982: Ground-level concentrations due to fumigation into an entraining mixed layer. *Atmos. Environ.*, **16,** 1159–1170.

——, and ——, 1984: Groundlevel concentration fluctuations from a buoyant and a non-buoyant source within a laboratory convectively mixed layer. *Atmos. Environ.*, **18,** 1297–1309.

——, and ——, 1985: Further results from a laboratory model of the convective planetary boundary layer. *Bound.-Layer Meteor.*, **32,** 205–236.

——, and ——, 1988: Concentration fluctuations within a laboratory convectively mixed layer. *Lectures on Air Pollution Modeling,* A. Venkatram and J. C. Wyngaard, Eds., Amer. Meteor. Soc., 357–384.

Du, S., J. D. Wilson, and E. Yee, 1994: Probability density functions for velocity in the convective boundary layer, and implied trajectory models. *Atmos. Environ.*, **28,** 1211–1217.

EPA, 1977: User's manual for single source (CRSTER) model. U.S. Environmental Protection Agency Rep. EPA-450/2-77-013, U.S. EPA, OAQPS, Research Triangle Park, NC, 285 pp.

——, 1987: Industrial Source Complex (ISC) dispersion model user's guide—Second edition (revised). Vol. 1. U.S. Environmental Protection Agency Rep. EPA-450/4-88-002a, U.S. EPA, OAQPS, Research Triangle Park, NC, 240 pp.

Fox, D. G., 1984: Uncertainty in air quality modeling. *Bull. Amer. Meteor. Soc.*, **65,** 27–36.

Garratt, J. R., J. C. Wyngaard, and R. J. Francey, 1982: Winds in the atmospheric boundary layer—Prediction and observation. *J. Atmos. Sci.*, **39,** 1307–1316.

Guillemet, B., H. Isaka, and P. Mascart, 1983: Molecular dissipation of turbulent fluctuations in the convective mixed layer. Part I: Height variations of dissipation rates. *Bound.-Layer Meteor.*, **27,** 141–162.

Hanna, S. R., 1984: The exponential probability distribution function and concentration fluctuations in smoke plumes. *Bound.-Layer Meteor.*, **29,** 361–375.

——, and R. J. Paine, 1989: Hybrid plume dispersion model (HPDM) development and evaluation. *J. Appl. Meteor.*, **28,** 206–224.

——, J. C. Weil, and R. J. Paine, 1986: Plume model development and evaluation, hybrid approach. Electric Power Research Institute Rep. D034-500, Electric Power Research Institute, Palo Alto, CA, 550 pp.

Henn, D. S., and R. I. Sykes, 1992: Large-eddy simulation of dispersion in the convective boundary layer. *Atmos. Environ.*, **26A,** 3145–3159.

Hicks, B. B., 1985: Behavior of turbulent statistics in the convective boundary layer. *J. Climate Appl. Meteor.*, **24,** 607–614.

Holtslag, A. A. M., and A. P. van Ulden, 1983: A simple scheme for daytime estimates of the surface fluxes from routine weather data. *J. Climate Appl. Meteor.*, **22,** 517–529.

Lamb, R. G., 1982: Diffusion in the convective boundary layer. *Atmospheric Turbulence and Air Pollution Modelling,* F. T. M. Nieuwstadt and H. van Dop, Eds., Reidel, 159–229.

Li, Z.-K., and G. A. Briggs, 1988: Simple pdf models for convectively driven vertical diffusion. *Atmos. Environ.*, **22,** 55–74.

Luhar, A. K., and R. E. Britter, 1989: A random walk model for dispersion in inhomogeneous turbulence in a convective boundary layer. *Atmos. Environ.*, **23,** 1911–1924.

——, and B. L. Sawford, 1995: Lagrangian stochastic modeling of the coastal fumigation phenomenon. *J. Appl. Meteor.*, **34,** 2259–2277.

Mason, P. J., 1992: Large-eddy simulation of dispersion in convective boundary layers with wind shear. *Atmos. Environ.*, **26A,** 1561–1571.

Misra, P. K., 1980: Dispersion from tall stacks into a shoreline environment. *Atmos. Environ.*, **14,** 397–400.

——, 1982: Dispersion of nonbuoyant particles inside a convective boundary layer. *Atmos. Environ.*, **16,** 239–243.

Moeng, C.-H., and J. C. Wyngaard, 1989: Evaluation of turbulent transport and dissipation closures in second-order modeling. *J. Atmos. Sci.*, **46,** 2311–2330.

Mylne, K. R., and P. J. Mason, 1991: Concentration fluctuation measurements in a dispersing plume at a range of up to 1000 m. *Quart. J. Roy. Meteor. Soc.*, **117,** 177–206.

Sawford, B. L., and F. M. Guest, 1987: Lagrangian stochastic analysis of flux–gradient relationships in the convective boundary layer. *J. Atmos. Sci.*, **44,** 1152–1165.

Sykes, R. I., 1988: Concentration fluctuations in dispersing plumes. *Lectures on Air Pollution Modeling,* A. Venkatram and J. C. Wyngaard, Eds., Amer. Meteor. Soc., 325–356.

——, W. S. Lewellen, and S. F. Parker, 1984: A turbulent-transport model for concentration fluctuations and fluxes. *J. Fluid Mech.*, **139,** 193–218.

——, ——, and ——, 1986: A Gaussian plume model of atmospheric dispersion based on second-order closure. *J. Climate Appl. Meteor.*, **25,** 322–331.

Taylor, G. I., 1921: Diffusion by continuous movements. *Proc. London Math. Soc., Ser. 2,* **20,** 196–212.

Turner, J. S., 1979: *Buoyancy Effects in Fluids.* Cambridge University Press, 368 pp.

Venkatram, A., 1982: A framework for evaluating air quality models. *Bound.-Layer Meteor.,* **24,** 371–385.

——, 1983: On dispersion in the convective boundary layer. *Atmos. Environ.,* **17,** 529–533.

——, 1988: Topics in applied dispersion modeling. *Lectures on Air Pollution Modeling,* A. Venkatram and J. C. Wyngaard, Eds., Amer. Meteor. Soc., 267–324.

Weil, J. C., 1988: Dispersion in the convective boundary layer. *Lectures on Air Pollution Modeling,* A. Venkatram and J. C. Wyngaard, Eds., Amer. Meteor. Soc., 167–227.

——, 1991: Appendix C: Discussion of lofting model and related dispersion models. Modification of hybrid plume dispersion model (HPDM) for urban conditions and its evaluation using the Indianapolis data set. Vol. II. Electric Power Research Institute Rep. A089-1200 II, Electric Power Research Institute, Palo Alto, CA, 160 pp.

——, 1990: A diagnosis of the asymmetry in top-down and bottom-up diffusion using a Lagrangian stochastic model. *J. Atmos. Sci.,* **47,** 501–515.

——, 1994: A hybrid Lagrangian dispersion model for elevated sources in the convective boundary layer. *Atmos. Environ.,* **28,** 3433–3448.

——, and R. P. Brower, 1983: Estimating convective boundary layer parameters for diffusion applications. Maryland Power Plant Siting Program Rep. PPSP-MP-48, Dept. of Natural Resources, Annapolis, MD, 37 pp.

——, and ——, 1984: An updated Gaussian plume model for tall stacks. *J. Air Pollut. Control Assoc.,* **34,** 818–827.

——, and L. A. Corio, 1985: Dispersion formulations based on convective scaling. Maryland Power Plant Siting Program Rep. PPSP-MP-60, Dept. of Natural Resources, Annapolis, MD, 39 pp.

——, ——, and R. P. Brower, 1986: Dispersion of buoyant plumes in the convective boundary layer. Preprints, *Fifth Joint Conf. on Applications of Air Pollution Meteorology,* Chapel Hill, NC, Amer. Meteor. Soc., 335–338.

——, R. I. Sykes, and A. Venkatram, 1992: Evaluating air-quality models: Review and outlook. *J. Appl. Meteor.,* **31,** 1121–1145.

Willis, G. E., and J. W. Deardorff, 1978: A laboratory study of dispersion from an elevated source within a modeled convective planetary boundary layer. *Atmos. Environ.,* **12,** 1305–1312.

——, and ——, 1981: A laboratory study of dispersion from a source in the middle of the convectively mixed layer. *Atmos. Environ.,* **15,** 109–117.

——, and ——, 1983: On plume rise within the convective boundary layer. *Atmos. Environ.,* **17,** 2435–2447.

——, and ——, 1987: Buoyant plume dispersion and inversion entrapment in and above a laboratory mixed layer. *Atmos. Environ.,* **21,** 1725–1735.

Wyngaard, J. C., 1988: Structure of the PBL. *Lectures on Air Pollution Modeling,* A. Venkatram and J. C. Wyngaard, Eds., Amer. Meteor. Soc., 9–61.